Potential Sources of Nitrous Acid (HONO) and Their Impacts on Ozone：A WRF-Chem study in a Polluted Subtropical Region

Li Zhang [1], Tao Wang [1,*], Qiang Zhang [2], Junyu Zheng [3], Zheng Xu [4,5], Mengyao Lv [6]

[1] *Department of Civil and Environmental Engineering, The Hong Kong Polytechnic University, Hong Kong, China*

[2] *Center for Earth System Science, Tsinghua University, Beijing 100084, China*

[3] *College of Environmental Science and Engineering, South China University of Technology, Guangzhou 510006, China*

[4] *Institute for Climate and Global Change Research & School of Atmospheric Sciences, Nanjing University, Nanjing, 210093, China*

[5] *Collaborative Innovation Center of Climate Change, Jiangsu Province, China*

[6] *National Meteorological Center, China Meteorological Administration, Beijing 100081, China*

[*] *Correspondence to: Tao Wang (cetwang@polyu.edu.hk)*

Key Points:

1. Comprehensive HONO sources are incorporated into WRF-Chem.
2. HONO from soil bacteria and oceans are important in forested and coastal areas.
3. The added HONO sources improved ozone predictions and increased 8-hourly maximum ozone.

Abstract

Current chemical transport models commonly under-simulate the atmospheric concentration of nitrous acid (HONO), which plays an important role in atmospheric chemistry, due to the lack or inappropriate representations of some sources in the models. In the present study, we parameterized up-to-date HONO sources into a state-of-the-art three-dimensional chemical transport model (WRF-Chem). These sources included (1) heterogeneous reactions on ground surfaces with the photo-enhanced effect on HONO production, (2) photo-enhanced reactions on aerosol surfaces, (3) direct vehicle and vessel emissions, (4) potential conversion of NO_2 at the ocean surface, and (5) emissions from soil bacteria. The revised WRF-Chem was applied to explore the sources of the high HONO concentrations (0.45-2.71 ppb) observed at a suburban site located within complex land types (with artificial land covers, ocean, and forests) in Hong Kong. With the addition of these sources, the revised model substantially reproduced the observed HONO levels. The heterogeneous conversions of NO_2 on ground surfaces dominated HONO sources contributing about 42% to the observed HONO mixing ratios, with emissions from soil bacterial contributing around 29%, followed by the oceanic source (~9%), photochemical formation via NO and OH (~6%), conversion on aerosol surfaces (~3%), and traffic emissions (~2%). The results suggest that HONO sources in suburban areas could be more complex and diverse than those in urban or rural areas and that the bacterial and/or ocean processes need to be considered in HONO production in forested and/or coastal areas. Sensitivity tests showed that the simulated HONO was sensitive to the uptake coefficient of NO_2 on the surfaces. Incorporation of the aforementioned HONO sources significantly improved the simulations of ozone, resulting in increases of ground-level ozone concentrations by 6-12% over urban areas in Hong Kong and the Pearl River Delta region. This result highlights the importance of accurately representing HONO sources in simulations of secondary pollutants over polluted regions.

Introduction

Nitrous acid (HONO) is an important source of the hydroxyl radical (OH)—the principal oxidant in the atmosphere—in the morning hours in polluted regions and thus has significant effects on secondary oxidation products such as ozone [*Alicke et al.*, 2003; *Kleffmann*, 2007; *Volkamer et al.*, 2010]. For a long time, the gas-phase reaction between nitric oxide (NO) and OH was considered to be the only important source of HONO during daytime hours. More recent field studies using newly available instruments have observed much higher daytime HONO concentrations than those calculated merely from the aforementioned gas-phase reaction in both rural and urban areas, implying a missing source or sources [*Kleffmann et al.*, 2005; *Li et al.*, 2014b; *Wong et al.*, 2013]. To explain the observed HONO levels, several production pathways for HONO have been proposed, including heterogeneous formation on humid surfaces, traffic emissions, gas-phase photolysis, and biological sources. The most commonly accepted new HONO source is the heterogeneous conversion from NO_2 to HONO on humid ground and particle surfaces, but whether the conversion mainly occurs on ground surfaces or on aerosol surfaces remains a subject of debate [*Kleffmann*, 2007]. A recent study observed faster conversions of NO_2 in air passing over the sea surface, suggesting that oceans may contribute to the production of HONO [*Zha et al.*, 2014]. Direct emission from vehicles has also been identified as a source of HONO, with a molar emission ratio of HONO to nitrogen oxide (NOx) ranging from 10^{-4} to 10^{-2} [*Kurtenbach et al.*, 2001]. Several new gas-phase formations of HONO have been proposed, including the photolysis of nitric acid [*Huber*, 2004], photolysis of ortho-substituted nitroaromatics [*Bejan et al.*, 2006; *Kleffmann*, 2007], reaction of photo-excited NO_2 with water vapor oxide [*Li et al.*, 2008], and reactions of NOx with hydrogen oxide radicals (HOx) (Note: the claim for the last source was later withdrawn) [*Li et al.*, 2014b; 2015; *Ye et al.*, 2015]. Emission from biological processes such as those of soil bacteria has been also suggested to be a potentially important source of HONO in forested regions [*Maljanen et al.*, 2013; *Oswald et al.*, 2013; *Su et al.*, 2011].

Earlier versions of chemical models only considered one or several homogenous pathways of HONO formation and thus gave low daytime HONO concentrations [*Lei et al.*, 2004; *Vogel et al.*, 2003]. More recent investigations incorporated additional direct and/or secondary HONO sources into models, which have improved simulations of HONO, ozone production, and secondary aerosols in polluted urban areas. *Sarwar et al.* [2008] included vehicle emissions, heterogeneous productions on ground and aerosol surfaces, and surface photolysis of absorbed HNO_3 into the CMAQ model and explained 60% of the averaged concentration of HONO observed in urban Philadelphia. Their modeling result suggested that the heterogeneous source on the ground was the dominant one (contributing ~36% to the observed HONO). *Li et al.* [2010] added similar sources and additional photo-dependent NO_2 heterogeneous reaction with semi-volatile organics into the WRF-Chem model, which significantly improved the simulation of HONO in Mexico City. Their results indicated that the NO_2 heterogeneous reactions with semi-volatile organics and on ground surfaces contributed 75% and 18% of the simulation, respectively, whereas the contribution from heterogeneous reaction on aerosol surfaces was negligible. *An et al.* [2011] and *Li et al.* [2011] considered the reaction of photo-excited NO_2 with water, vehicle emissions, and heterogeneous reactions on aerosols in WRF-Chem and reproduced 72% and 55% of the observed HONO in urban Beijing, respectively. They suggested that the heterogeneous reaction of NO_2 on aerosol surfaces was the largest contributor to the simulated HONO concentration. Similar sources with the photo-enhanced formation on ground surfaces were parameterized into CMAQ by *Czader et al.* [2012] which improved the HONO observed at different altitudes in urban Houston and suggested that the formation on surfaces was the most important source of HONO. By including vehicle emissions and heterogeneous sources on ground and aerosol surfaces, *Gonçalves et al.* [2012] explained about 45% of the mean observed HONO concentration in urban Spain.

Despite advances in the understanding of HONO sources, uncertainties remain in representing them in the current state-of-the-art models. Because the exact mechanisms of the non-gaseous HONO pathways are still not well understood, parameterizations of these sources in the models are highly simplified with large variations in key parameters adopted by different modeling studies. Heterogeneous production on wet surfaces has been treated as a first-order process with the reaction rate proportional to the uptake coefficient of NO_2 (γ_{NO_2}). Laboratory-determined γ_{NO_2} so far varies significantly for different surfaces and from different experimental set-ups. The majority of lab experiments have suggested a γ_{NO_2} in the range of 10^{-7}-10^{-5} on surfaces of organics, dust, soot, and inorganic acid [*Ammann et al.*, 2005; *George et al.*, 2005; *Kleffmann et al.*, 1998; *Monge et al.*, 2010; *Ndour et al.*, 2008; *Wong et al.*, 2011] and of 10^{-6}-10^{-5} on ground surface [*Kurtenbach et al.*, 2001; *VandenBoer et al.*, 2013]. However, several other studies reported much larger values of 10^{-4}-10^{-3} on lab-generated droplets and aerosols, which were attributed to catalytic reactions by inorganic and organic anions [*Colussi et al.*, 2013; *Yabushita et al.*, 2009]. It is unclear whether these large values are applicable to atmospheric conditions due to the different compositions of droplets/aerosols used in the experiments and those encountered in the real atmosphere. Previous modeling investigations of HONO adopted a γ_{NO_2} on aerosol surfaces varying on the order of 10^{-6} to 10^{-4}, leading to different conclusions on the importance of aerosols in HONO formation [*An et al.*, 2013; *Aumont et al.*, 2003; *Li et al.*, 2010; *Li et al.*, 2011; *Sarwar et al.*, 2008]. Other uncertainties in simulating HONO concentrations in current chemical transport models arise from the lack of representations of emissions from soil microbial processes and the conversion of NO_2 on the ocean surface, yet these sources/processes could be important in rural and coastal areas.

In the present study, up-to-date HONO sources, including the recently proposed gaseous formations, emissions from soil bacteria, and heterogeneous formations of HONO on ocean, aerosols, urban, and vegetation surfaces, are incorporated into a widely used regional chemistry transport model (WRF-Chem). The revised WRF-Chem model is applied to simulate the HONO sources at a suburban site in Hong Kong during a multiday photochemical episode when the HONO levels reached 1-3 ppb. The main goals of this study are to explore the potential source or sources of such high levels of HONO measured at the suburban site and their effects on regional ozone concentrations over the Hong Kong and Pearl River Delta region (HK-PRD).

2. Methodology

2.1. WRF-Chem Model and Configurations

The three-dimensional Weather Research and Forecasting model coupled with Chemistry (WRF-Chem, version 3.4.1), which simulates the transport, mixing, and chemical transformation of trace gases and aerosols simultaneously with meteorology [*Grell et al.*, 2005], was applied in this study. The chemical mechanism used to simulate concentrations of gases and aerosols is based on the Carbon-Bond Mechanism version Z (CBMZ) [*Zaveri and Peters*, 1999] coupled with the 4-bin sectional Model for Simulating Aerosol Interactions and Chemistry (MOSAIC) [*Zaveri et al.*, 2008]. The CBMZ gas-phase mechanism treats 67 species and 164 reactions using a lumped-structure approach that categorizes organic compounds according to the types of bonds present in their molecular structures. MOSAIC considers sulfate, nitrate, chloride, carbonate, ammonium, methanesulfonate, sodium, calcium, black carbon (BC), primary organic carbon (OC), liquid water, and other inorganic mass within 4 size bins ranging between 3 nm and 10 μm. Aqueous-phase chemistry based on the work of *Fahey and Pandis* [2001] was used. Other major physical and chemical schemes adopted in this study are listed in Table 1. Aerosol-meteorology interactions in the model were turned off. Three two-way nested modeling domains were used with the horizontal resolution of the three nested domains being 27, 9, and 3 km, respectively. The outermost and innermost domains covering the PRD region and Hong Kong are illustrated in Figure 1. The vertical resolution includes 31 layers with a fixed-model top pressure of 100 hpa, and the first layer is set to be about 35 m above ground surface. Initial and boundary conditions for WRF-Chem were provided by the simulations of MOZART-4 driven by GEOS-5 fields [*Emmons et al.*, 2010]. The simulation period was 19-31 August 2011, with the first 32 hours considered as a spin-up time.

A multiscale assimilation method combining observational and analytical nudging was used throughout the simulation period. This method has been found to effectively improve the meteorological performance of WRF-Chem by *Zhang et al.* [2015]. Meteorological observations at 2513 surface stations (tri-hourly) and 251 sounding stations (12-hourly) were obtained from the China Meteorological Administration and integrated in the simulations through observational nudging (Figure 1a). Hourly surface observations at 40 weather stations in Hong Kong were also assimilated (Figure 1b). NCEP final reanalysis data was used in analytical nudging. Details of the method are given in *Zhang et al.* [2015]. The meteorological predictions were evaluated following *Zhang et al.* [2015], which shows satisfactory model performances (Table S1).

Four sets of anthropogenic emission inventories covering different regions were applied (Table 2) for the three nested model domains used in our simulations. For the outmost domain, the Multi-resolution Emission Inventory for China (MEIC) in 2010, covering mainland China, was used. The MEIC inventory, containing monthly anthropogenic emissions of SO_2, NO_X, CO, NH_3, $PM_{2.5}$, PM_{coarse}, BC, OC, and non-methane volatile organic compounds (NMVOCs) in five sectors (agriculture, industry, power plants, residential, and transportation), was developed by Tsinghua University based on a technology-based emission model [*Lei et al.*, 2011; *Zhang et al.*, 2009b]. It was used to simulate the $PM_{2.5}$ in multiple cities around China in 2010-2014 and found to provide reasonable results [*Zhang et al.*, 2015]. For other Asian regions, we used the 2006 INTEX-B emission inventory [*Zhang et al.*, 2009b]. For the PRD region, we used a more recent inventory of 2010 with a fine resolution of 3 km developed by the South China University of Technology. This emission inventory contains major pollutants including CO, NO_X, SO_2, PM_{10}, $PM_{2.5}$, and NMVOCs in agriculture, power plant and industry, residential, river and marine vessel, and vehicle transportation sectors. The 2010 emission inventory for Hong Kong was developed by the Hong Kong Environmental Protection Department (HKEPD), comprising the emissions for CO, NO, SO_2, BC, OC, sulfate, nitrate, ammonium, and NMVOCs in the power plant, industry, residential, marine vessel, aviation, and on-road transportation sectors. NMVOCs in the PRD and Hong Kong were mapped into the CBMZ chemical mechanism by using a similar approach to that in *Li et al.* [2014a]. Seasonal variations derived from the MEIC were applied to the other three inventories. Diurnal, day-of-week, and vertical allocations of the emissions were the same as in *Zhang et al.* [2015]. Biogenic emissions were estimated online by the Model of Emissions of Gases and Aerosols from Nature (MEGAN v2.01) [*Guenther et al.*, 2006].

2.2. Additional Sources of HONO

The CBMZ chemical mechanism in WRF-Chem does not contain any direct emissions or secondary pathways of HONO except for the well-known homogeneous formation via OH and NO. In this work, the following new sources of HONO were added into the model and evaluated through sensitivity simulations.

2.2.1. Heterogeneous sources on ground and aerosol surfaces

To consider the potential heterogeneous sources of HONO from ground and aerosol surfaces, we included the following reactions involving HONO proposed in previous studies into WRF-Chem:

$$\mathrm{NO} + \mathrm{HNO_3} \xrightarrow{surface} \mathrm{HONO} + \mathrm{NO_2} \qquad \text{(R1) } k_1$$

$$\mathrm{NO} + \mathrm{NO_2} + \mathrm{H_2O} \xrightarrow{surface} \mathrm{2HONO} \qquad \text{(R2) } k_2$$

$$\mathrm{2HONO} \xrightarrow{surface} \mathrm{NO} + \mathrm{NO_2} + \mathrm{H_2O} \qquad \text{(R3) } k_3$$

$$\mathrm{2NO_2} + \mathrm{H_2O} \xrightarrow{aerosol\ surface} \mathrm{HONO} + \mathrm{HNO_3} \qquad \text{(R4) } k_a$$

$$\mathrm{2NO_2} + \mathrm{H_2O} \xrightarrow{ground\ surface} \mathrm{HONO} + \mathrm{HNO_3} \qquad \text{(R5) } k_g$$

The reaction rates for reactions R1-R3 were obtained from *Foley et al.* [2009]. The first-order reaction rate for R4 is estimated following the recommendations in *Li et al.* [2010] as follows:

$$\mathrm{k_a} = \frac{1}{4} \cdot v_{\mathrm{NO_2}} \cdot \left(\frac{S_a}{\mathrm{V}}\right) \cdot \gamma_{\mathrm{a-NO_2}} \qquad (1)$$

where $v_{\mathrm{NO_2}}$ is the mean molecular velocity of NO_2 (m s^{-1}), S_a/V is the aerosol surface to volume ratio (m^{-1}) representing the surfaces available for heterogeneous reaction, and γ_{a-NO_2} is the uptake coefficient of NO_2 at the aerosol surface. γ_{a-NO_2} was set to be 1×10^{-6} for nighttime [*Aumont et al.*, 2003; *Kurtenbach et al.*, 2001]. It has been reported that sunlight dramatically boosts the conversion of NO_2 into HONO on the surfaces of organics, soot, and dust [*George et al.*, 2005; *Monge et al.*, 2010; *Ndour et al.*, 2008; *Stemmler et al.*, 2006]. To consider this photo-enhancing effect, we applied a higher value of 2×10^{-5} for γ_{a-NO_2} during the daytime when the light intensity was lower than 400 W m^{-2}, whereas we linearly scaled it with solar radiation when the light intensity was higher than 400 W m^{-2} (equation 2).

$$\gamma_{a-NO_2} = 2 \times 10^{-5} \cdot \left(\frac{\text{light intensity}}{400}\right) \qquad (2)$$

S_a is the total aerosol surface per volume of air and is calculated by the MOSAIC aerosol module in WRF-Chem. The reaction rate at the ground surface is calculated by equation 3 following the method in *Li et al.* [2010]:

$$k_g = \frac{1}{8} \cdot v_{NO_2} \cdot \left(\frac{S_g}{V}\right) \cdot \gamma_{g-NO_2} \qquad (3)$$

where S_g/V represents the ground surface to volume ratio, and γ_{g-NO_2} is the uptake coefficient of NO_2 at the ground surface, which we assume to be the same as that for aerosol surfaces and is calculated by applying the method described in *Li et al.* [2010]. Over the urban areas as defined by the MODIS land-use data, we adopted a constant S_g/V value of 0.3 m^{-1}. For the vegetation-covered areas, the leaf area index (LAI, m^2/m^2) was used to estimate the surface area to volume ratio (equation 4) following the method in *Sarwar et al.* [2008]:

$$\frac{S_g}{V} = \frac{2 \times LAI}{H} \qquad (4)$$

where H is the height of the first model layer, and LAI is multiplied by a factor of 2 to take account of the areas on both sides of the leaves [*Sarwar et al.*, 2008; *Zhang et al.*, 2012]. Since the LAI can vary significantly with the seasons, 8-day averages of MODIS-measured LAI during 21-29 August 2011 at a resolution of 0.1° were used to represent the mean condition during our simulation period (data was obtained from NASS at http://neo.sci.gsfc.nasa.gov/). The heterogeneous conversion of NO_2 on the ground surface was only considered within the first model layer, whereas that on the aerosol surface was treated in all model layers. In view of the fact that a wide range of uptake coefficients of NO_2 have been adopted in other studies as discussed previously, we conduct sensitivity tests to evaluate the impacts of different uptake coefficients on the simulated HONO in section 3.3.

2.2.2. Direct traffic emissions

HONO to NO_X ratios in vehicle exhausts are found within a range of 0.29-1.7% [*Kirchstetter et al.*, 1996; *Kurtenbach et al.*, 2001; *Rappenglück et al.*, 2013; *Xu et al.*, 2015], and a ratio of 0.8% has been commonly used in previous modeling studies [*Gonçalves et al.*, 2012; *Sarwar et al.*, 2008]. In our study, we applied an emission ratio of 0.8% for gasoline vehicles in our emission inventories and 2.3% for the diesel vehicles to take account of the promotion of HONO formation by semi-volatile organics in diesel exhausts [*Gutzwiller et al.*, 2002]. All marine and river vessels were assumed to use diesel engines and hence were applied the same emission factor as diesel vehicles. Figure 2a illustrates the hourly emission of HONO for the transport sector over the HK-PRD region on a weekday. In view of large variations in the traffic emission factor of HONO, in Section 3.3, we conduct sensitivity runs to test different emission ratios.

2.2.3. Heterogeneous source from sea surface

Zha et al. [2014] recently reported a NO_2-to-HONO conversion rate of $3.17\text{-}3.36\times10^{-2}$ h^{-1} in air masses passing over sea surfaces, which is almost three times the rate over land surfaces ($1.20\text{-}1.30\times10^{-2}$ h^{-1}), at a clean coastal site in Hong Kong. Although the exact mechanism is not yet clear, formation of HONO on the ocean surface could be a non-negligible contributor to atmospheric HONO in areas adjacent to the ocean such as Hong Kong. In previous modeling studies, sea surface has usually been considered as a sink rather than a source of HONO. The only study treating sea surface as a source was that by *Elshorbany et al.* [2012], who used a uniform ratio of HONO/NOx over land and sea in a global model. In the present study, a NO_2-to-HONO conversion rate of 3.17×10^{-2} h^{-1} is adopted over the ocean surface in the first model layer of WRF-Chem to consider this possible oceanic source in a regional model for the first time.

2.2.4. Direct emissions from soil bacteria

It has been proposed that direct releases from soil in equilibrium with nitrite could be an important source of atmospheric HONO in natural and agricultural areas [*Maljanen et al.*, 2013; *Oswald et al.*, 2013; *Su et al.*, 2011]. *Maljanen et al.* [2013] took soil cores samples from 11 boreal ecosystems and measured the production rates of HONO, NO, and N_2O from the soils in the laboratory and found that HONO emission peaked in drained boreal peatlands, which cover a large area over the Northern Hemisphere. *Oswald et al.* [2013] investigated soil samples collected from various ecosystem across the world and showed that ammonia-oxidizing bacteria emit HONO in unexpectedly large quantities from different soil types, which might account for up to 50% of the reactive nitrogen released from soils. To the best of our knowledge, this potentially important source has not been considered in any previous global or regional models. In this study, the emissions of HONO from soil bacteria with consideration of the dependence on land category, soil humidity, and temperature were parameterized into WRF-Chem. To do this, we first mapped the soil categories measured in *Oswald et al.* [2013] (collected from 17 ecosystems in Table S2) into the most closely matching USGS land categories in the WRF-Chem model following the mapping schemes described in Table S3 in the supplementary materials. The optimum emission flux for each USGS land-use type was then calculated as the aggregation of the measured fluxes from the measured category/categories that was/were mapped into the specific USGS classifications (Table S3). After that, the optimum fluxes over the nested domains were digested into the model and further scaled online according to the soil temperature and water content in each model grid at each time step throughout the simulation period by the following equation:

$$F_N(HONO) = F_{N,opt}(HONO) \cdot e^{\frac{E_a}{R} \cdot \left(\frac{1}{T_{opt}} - \frac{1}{T}\right)} \cdot f(SWC) \qquad (5)$$

where $F_{N,opt}$ is the optimum flux of HONO in terms of N, E_a is the activation energy for HONO, which is set to be 80 kJ mol^{-1}, R is the gas constant, T_{opt} is the temperature at which optimum flux is emitted and is 298.15 K in the experiments of *Oswald et al.* [2013], T and SWC are the soil temperature and soil water content, respectively, which are estimated by WRF online, and $f(SWC)$ is a scaling function related to soil water content and is fitted based on the data curves in Figures 1 and 3 in *Oswald et al.* [2013]. Figure 2b gives an example of the optimum emission flux of bacterial HONO from soil over our innermost model domain. It should be noted that large uncertainties may exist in the parameterization of soil emission of HONO due to the limited number of measured soil types, ignorance of the differences between the soil categories measured in *Oswald et al.* [2013] and those in the model, and relatively simple treatments of the dependences of soil water content and temperature.

2.2.5. Gas-phase formation

As previously discussed, several gas-phase formation pathways of HONO have been proposed, including the reaction of photo-exited NO_2 with water vapor and photolysis of gas-phase nitric acid. However, modeling studies indicate that these two sources are of minor importance due to small rate constants [*Huber*, 2004; *Tyndall et al.*, 1995]. Our simulations also confirmed the negligible contributions of these sources (results not shown), and thus they were not considered in the revised WRF-Chem model. For HONO production from the photolysis of organic nitrates, due to insufficient information on their reaction rates, it is difficult to quantify these sources in numerical models at present [*Kleffmann*, 2007]. Therefore, they were not included in our revised model. For the new gas-phase source via the reaction between NOx and HOx proposed by *Li et al.* [2014b], we have added a series of reactions shown in Table S4 to test its importance at our study site.

2.2.6. Simulation cases

Seven simulation cases were designed as listed in Table 3, including: (1) BASE case: only considering the default photochemical reaction of OH and NO; (2) L case: with additional heterogeneous sources of HONO from land surfaces; (3) LO case: similar to L, but considering the potential source from the ocean surface; (4) LOA case: similar to LO, but with the heterogeneous source at the aerosol surface in all vertical model layers; (5) LOAE case: similar to LOA, but with direct emissions of HONO from transportation added; (6) LOAES: similar to LOAE, but including parameterized emissions of HONO from soil bacteria into the model with consideration of land type, temperature, and soil water content; and (7) LOAESG: similar to LOAES, but including additional gas-phase formation.

2.3 Field measurements

Field measurements of HONO and many other chemical constituents were conducted at the Tung Chung (TC) air-quality monitoring station in Hong Kong. The present study used the data over the period of 20-31 August 2011, during which a severe multiple-day episode occurred in the region. The TC site (22.30°N, 113.93°E, Figure 3) is located in a residential suburban area in the northern part of Lantau Island and is surrounded by the South China Sea in the north, Hong Kong International Airport in the northwest, and vegetation-covered hilly areas on other sides. A detailed description of the site and the surroundings can be found in [*Xu et al.*, 2015]. HONO was measured using a commercial long-path absorption photometer (model LOPAP-03, QUMA) [*Heland et al.*, 2001; *Kleffmann and Wiesen*, 2008]. NO and NO_2 concentrations were measured with a chemiluminescence instrument (model 42i, TEI) coupled with a photolytic converter (model BLC, Droplet Measurement Technologies). CO was measured using a nondispersive analyzer (model 300, API). $PM_{2.5}$ was measured by a tapered-element oscillating microbalance (TEOM 1405-DF, Thermo Scientific) with a Filter Dynamic Measurement System, and the particle number and size distribution in the range of 5 nm to 10 μm were measured with a wide-range particle spectrometer (model 1000XP, MSP Corporation). The total aerosol surface density was calculated based on the measured particle number size distributions by assuming the particles to be ideal spheres. O_3 was measured by a UV photometric analyzer (model 49i, TEI), and the same instrument and method were applied by the HKEPD to measure the O_3 levels at other air-quality monitoring stations over Hong Kong (Figure 3). All instruments were set up on the roof of the 4-story Tung Chung Health Center with sample inlets installed at ~20 m above ground level, whereas the LOPAP-03 sampling unit was installed at ~15 m above ground level.

3. Results and Discussion

3.1. The severe episode

Figure 4 shows the observed and simulated (BASE and LOAES cases) concentrations of several major pollutants (CO, NO_2, SO_2, and $PM_{2.5}$) at the TC site. During 20-24 August, the PRD and Hong Kong were south of low-pressure systems that created predominated southerly winds, which brought in relatively clean air masses from the ocean (Figure S1a). Consequently, the observed mean concentrations of CO, NO_2, SO_2, and $PM_{2.5}$ were only 138.9 ppb, 14.7 ppb, 3.2 ppb, and 8.5 μg m^{-3}, respectively during this period. After that, the winds abruptly changed to northerly, and the concentrations of all major pollutants surged by 4-6 times as shown in Figure 4 and remained at high levels during 25-31 August. The maximum hourly ozone concentrations were 80-160 ppb over Hong Kong, with high concentrations also observed in the upwind stations such as Yuen Long and Tai Po (see results in section 3.4). The simulated results shown in Figure 4 indicate that the model well captured the concurrent sharp increases in the pollutants' levels. It is worth noting that CO and SO_2, which are less related to HONO chemistry, had negligible discrepancies in different simulated cases (Figure 4).

Surface weather charts (Figure S1) showed that this severe episode was associated with a strong typhoon (Super Typhoon Nanmadol). As Nanmadol moved closer to the South China Sea (Figure S1b), the PRD region, which is to the northwest of the typhoon, was affected by the anticlockwise circulation of typhoon with northerly winds. Consequently, large amounts of pollutants were continuously transported downwind from the highly industrialized PRD region to Hong Kong. Meanwhile, the typhoon caused downward motions over the region due to the large-scale subsidence at its outskirts [*Ding et al.*, 2004; *Lam et al.*, 2005], and as a result, the PRD experienced strong solar radiation and high temperature (see measurements at TC in Figure S2), facilitating photochemical formations of ozone. Besides, the subsiding air motion resulted in a shallow boundary layer over Hong Kong (Figure S3) favoring the build-up of the pollutants.

3.2. HONO measurements and simulations

Figure 5 illustrates the observed and simulated HONO in each case during the study period. Before the episode, measured HONO levels were at 200-1500 ppt. After August 25, the HONO abruptly increased to 1-3 ppb along with the concurrent jump in other pollutants. As depicted, with only the HONO source from NO + OH, the BASE case underestimated the concentration by a factor of 10-100 (Figure 5), which is similar to the findings in previous modeling studies [*Gonçalves et al.*, 2012; *Li et al.*, 2010; *Li et al.*, 2011]. With the consideration of the heterogeneous conversion of NO_2 on land surfaces, the simulated HONO in the L case increased the HONO level by almost an order of magnitude (Figures 5 and 6). The oceanic source in the LO case further increased the averaged HONO from 386 ppt in the L case to 466 ppt. Figure S4a shows the differences between the L and LO cases, which indicates that the oceanic source contributed more than 100 ppt of HONO over the immediate coastal areas along eastern China. Compared with the LO case, adding the heterogeneous source on aerosol surfaces only enhanced the HONO by 28 ppt on average, whereas the direct traffic emissions led to an increase of 18 ppt in mean HONO in the LOAE case (compared with the LOA case).

Including emissions from soil bacteria from vegetation-covered surfaces in the LOAES case further narrowed the gap between the modeled and observed HONO (Figures 5 and 6). Compared with the results in the LOAE case, this newly-added source increased the simulated HONO by 266 ppt on average with a minimum daily increase of 95 ppt on 28 August and a maximum increase of 373 ppt on 30 August. Since the soil bacteria emission in the model grid where TC is located is zero, the HONO from soil bacteria at TC was mainly transported from surroundings and thus the wind directions and speeds would significantly affect the contributions of this source at TC. Besides, compared with daytime, the lifetime of HONO was much longer during nighttime and thus the "soil" HONO can be continuously transported from surrounding source regions. As shown in Figure 2b, TC is surrounded by large HONO emissions from soil bacteria in the northeast and west. So during the nighttime of 20 and 21 August, large contributions from soil occurred when weak northeasterly and westerly winds dominated (Figure S2). Similarly, during the nighttime of 29 and 30 August, westerly winds transported large amounts of HONO to TC from source regions in the west and the HONO accumulated there. In contrast, when the northwesterly winds dominated, less "soil" HONO were transported from the urban areas of PRD to TC (Figure S2). Figure S5a also suggests that emissions from soil bacterial can be a substantial HONO source over the areas covered by or adjacent to vegetation and soil lands.

In the LOAESG case, the gas-phase source via reactions between $HO_2 \cdot H_2O$ and NO_2 significantly enhanced the simulated HONO concentrations especially at noon and during the nighttime (Figures 6 and 7). Overall, this source did slightly improve the HONO simulation during the daytime, supporting the suggestion of a potential NOx-consuming gas-phase source [*Li et al.*, 2015]. However, *Ye et al.* [2015] pointed out that the assumption of a HONO yield of 100% from the reactions between $HO_2 \cdot H_2O$ and NO_2 (Table S4) is inappropriate (i.e., the yield is too high). As the exact mechanism of this NOx-consuming gas-phase formation has not been identified [*Li et al.*, 2015], we do not consider it hereafter. On average, the LOAES, LOAE, LOA, LO, L, and BASE cases reproduced 85%, 56%, 54%, 51%, 42%, and 6% of the observed HONO, respectively (Figure 7).

The sources included in the comprehensive LOAES case could explain 65% of the observed daytime HONO concentrations. The underestimate of HONO might be due to several reasons. First, our model underestimated a main precursor of HONO, NO_2, in the daytime by 31% (Figure S6a). As described in section 2.3, our measurement site is close to the TC expressway and the airport. Due to the relatively low model resolution (3×3 km), the traffic emission of NOx was averaged into the grid where TC is located, and thus the model under-simulated the concentration of NO_2 at TC. Secondly, the direct emissions of HONO from traffic might also be underestimated at the TC site in the model. A third reason for the under-simulation of HONO might be that there are some missing daytime sources that we have not considered or adequately accounted for in our model. The uncertainty in each source and possible missing HONO processes are discussed later in section 3.3.

With the adopted parameters, our model results suggest that the heterogeneous conversion of NO_2 on land surface was the dominant source (~42%) of the HONO observed at the TC site as shown in Figure 7b, and this conclusion is similar to those inferred in previous field measurements [*Kleffmann et al.*, 2003; *Li et al.*, 2012; *Michoud et al.*, 2013; *Zhang et al.*, 2009a] and from modeling studies [*Czader et al.*, 2012; *Sarwar et al.*, 2008; *Zhang et al.*, 2012]. The second largest source of HONO was the emission from soil bacteria, which contributed around 23% to the observed HONO on average. The oceanic source and the gaseous formation via photochemical reaction consuming OH and NO contributed approximately 9% and 6% of the mean HONO concentration, respectively, whereas the heterogeneous reaction on aerosol surfaces only contributed about 3% (Figure 7b). The important contributions from soil bacteria and from conversion of NO_2 on the ocean surface were illustrated for the first time in our study. The finding on a small contribution from aerosol is consistent with those in many previous modeling studies, which can be explained by the fact that aerosol surface areas are generally much smaller than ground surface areas and therefore should be much less effective in producing HONO via the heterogeneous reaction compared to the ground surface [*Aumont et al.*, 2003; *Li et al.*, 2010; *Sarwar et al.*, 2008; *Vogel et al.*, 2003].

3.3 Uncertainties in the HONO simulations by the revised WRF-Chem model

3.3.1 Uncertainties in heterogeneous conversions of NO_2 on land and aerosol surfaces

The production rates of HONO on the surface (R4 and R5) are affected by the surface area to volume ratio (S/V) and the uptake coefficient of NO_2 (γ_{NO_2}) on surfaces (Equations 1 and 3), both of which are subject to uncertainties. The ground surface area to volume ratio (S_g/V) strongly depends on the physical properties of land covers, and values in the range of 0.1-0.3 m^{-1} have been used in previous studies on urban surfaces [*Li et al.*, 2010; *Svensson et al.*, 1987; *Vogel et al.*, 2003]. *Sarwar et al.* [2008] used a value of 0.3 for urban model grids and scaled the value according to the percentage of urban area in each model grid. A value of 0.3 m^{-1} over urban areas used in our study is comparable with the ones suggested in previous modeling studies and is believed to be reasonable as the mega-cities in PRD such as Guangzhou and Hong Kong are highly urbanized. For the vegetation-covered areas, we used the LAI to estimate the S_g/V, which is a more accurate way than applying a constant value over the whole model domain. The surface to volume ratio of aerosols (S_a/V), in the range of 10^{-4}-10^{-3} in a typical polluted urban atmosphere of China [*Gao et al.*, 2009; *Liu et al.*, 2012], is much smaller than that of the ground surface, and in our case, the model calculated S_a/V to be 3.86×10^{-4} m^{-1} on average (slightly smaller than the observed value of 6.25×10^{-4} m^{-1}). We conducted a sensitivity test by doubling the aerosol surface area in the MOSAIC module, which only led to an increase of 10.1 ppt in mean HONO concentration, indicating that the simulated HONO is not sensitive to the aerosol surface area density at TC (figures not shown).

In comparison, γ_{NO_2} has a much wider range, with measurement-derived values from 10^{-7} to 10^{-3} on different surfaces, and the values of 10^{-6} to 10^{-4} have been used in previous modeling studies. Therefore, the choice of this parameter would have a large effect on the model assessment of importance of a heterogeneous source of HONO. In our study, the four sensitivity tests listed in Table 4 were conducted: use of a relatively large γ_{NO_2} of 1×10^{-4} on land surfaces (LOAES_LL) and on aerosol surfaces (LOAES_AL); use of a smaller γ_{NO_2} of 1×10^{-6} on land surfaces (LOAES_LS) and on aerosol surfaces (LOAES_AS). Due to limited computation sources, these sensitivity runs were performed over the outermost domain (Domain 1) at a resolution of 27×27 km and were based on the comprehensive LOAES case. As illustrated in Figure 8, the simulated HONO in LOAES_LS and LOAES_AS, that is, using the smaller uptake coefficient, had small discrepancies (-14% and -15%, respectively) compared with the results in LOAES. However, using a larger γ_{NO_2} (in LOAES_LL and LOAES_AL) led to an unrealistic overestimate in the nighttime HONO by a factor of 3-6 because of the adoption of a γ_{NO_2} two orders of magnitude larger than that used in the LOAES case at nighttime. The changes in HONO during noontime (10:00-14:00 LTC) were unnoticeable because the photo-enhancing scaling factor used to calculate the daytime γ_{NO_2} could increase by a factor of 2.5 at the TC site according to Equation (2) when the simulated solar radiation varies from 0 to around 1000 W/m^2 during the daytime. In summary, based on the available experimental data and the simulation results in our study, we believe that our choice of the values of γ_{NO_2} for ground and aerosol surfaces could be reasonable.

3.3.2. Uncertainties in direct traffic emissions

Two sensitivity runs were conducted with the use of different traffic emission ratios (see Table 4). The LOAESG_2E case doubled the direct emissions of HONO from transportation, and in LOAESG_TCE we applied an empirical relationship between the emission ratio of HONO/NO_X and BC derived from the measurements at the TC site by *Xu et al.* [2015] as follows:

$$\frac{E_{HONO}}{E_{NO_X}} = 0.0050 + 0.003 \times E_{BC}\ (\mu g\, m^{-2}\, s^{-1}) \cdot \tau\ (s)/H(m), \qquad (6)$$

where E_{HONO}, E_{NO_X}, and E_{BC} are the emission intensities of HONO, NO_X, and BC in the transportation sectors of emission inventories, respectively, τ is the emitting time and is assumed to be 3600 s, and H is the height of first model layer (~35 m).

As shown in Figure 9, the doubling of traffic emissions led to slight increases in the diurnal HONO levels, with a larger enhancement of 21.2-24.9 ppt during morning rush hours (05:00-08:00 LTC) and a negligible increase during 10:00-15:00 LTC due to the stronger photolysis of HONO during that period. Compared with LOAESG, the mean daily change in LOAESG_2E was only 10.4 ppt (1.7%). However, the HONO level was slightly lower in LOAES_TCE due to a smaller averaged emission ratio of 0.6% over our simulation domain. Overall, the simulated HONO concentrations at suburban TC, with discrepancies ranging from -1.6% to 7.0% between the different cases, were not sensitive to the emission ratio of HONO from transportation. This result is different from that in *Czader et al.* [2015] in urban Houston. In their study, doubling the traffic emission ratio to 1.6% which was close to the measurement-derived ratio of 1.7% in the city [*Rappenglück et al.*, 2013] significantly increased the simulated HONO by 36% at a urban site in Houston.

3.3.3. Uncertainties in emissions from soil bacteria

Large uncertainties may exist in the parameterization of soil emissions of HONO. One has to do with the mapping of limited soil types for which emission fluxes have been measured in *Oswald et al.* [2013] into the land categories that are used in the model. To assess the uncertainties with this process, two sensitivity runs, LOAES_SMAX and LOAES_SMIN using the soil types that have the maximum or the minimum emission flux within the ones mapped into each model land category, were performed (Table S3). The simulated HONO in these two sensitivity runs only had -10% to 9% changes compared with the result in the LOAES case during the early morning (Figure S7). Another uncertainty may come from the relatively simple treatments of the dependences of HONO emission on soil water content and temperature. In addition, the emission fluxes from soils measured in the laboratory may not accurately represent those in the real environment as the emitting processes vary with nutrient contents in soils over regions and are potentially influenced by background HONO concentration in the atmosphere [*Oswald et al.*, 2013]. Additional measurements of emission fluxes under different soil humidity and temperature for soil samples collected in various ecosystems are needed to further refine the treatment of this source of HONO.

3.3.4. Possible ignorance of other potential processes of HONO

Our modeling results show that the HONO level was slightly overestimated during midnight (23:00-03:00 LTC) in the LOAES case (Figure 6). This might be due to insufficient account of the uptake of HONO by the ground surface, which could be an important sink for HONO but received little consideration [*Donaldson et al.*, 2013; *VandenBoer et al.*, 2014]. The HONO concentrations during the early morning (04:00-07:00 LTC), on the other hand, were underestimated by 50%-70% despite that NO_2 was well simulated as illustrated in Figure S6a. For daytime, the HONO and NO_2 values during 08:00-11:00 were well simulated (Figure 6 and Figure S6a). Therefore, the underestimates of HONO during the early morning are unlikely due to the imperfect representation of its main heterogeneous sources. Several previous studies suggest that gaseous HONO could be released from the surface during the morning in response to chemical and physical changes such as the evaporation of dew, release from soil pore water, and/or bacterial processes [*He et al.*, 2006; *Rubio et al.*, 2008; *Rubio et al.*, 2009]. Dew water can serve as a reservoir of HONO during the nighttime and as a source in the morning with the evaporation of dew droplets. It can be seen in Figure S6b that the RH did peak during that period presumably from the evaporation of dew droplets and/or soil water. Therefore, there is likely a source of emission of HONO from dew evaporations, and our tests in Figure S8 suggest that this emission flux is within a range of 100-500 $ng/m^2/s$ at the TC site.

3.4 Effects on ozone

3.4.1. Improvement of ozone predictions over Hong Kong

We next assessed the effects of adding the additional HONO sources in WRF-Chem on the simulated ambient ozone concentrations in the HK-PRD region. Because LOAES case reproduced HONO observations fairly well, the evaluations were carried out based on this case. Figure 10a and b show the differences in simulated O_3 and OH at the TC site between the LOAES and BASE cases, respectively. HONO built up during the nighttime and quickly was photolyzed into OH after sunrise. As a result of the much higher level of HONO in the LOAES case, daytime OH increased by 86% at the TC site (from 0.07 ppt in the BASE to 0.13 ppt in the LOAES case, on average). Similar increases in simulated OH (50%-100%) were suggested in *Aumont et al.* [2003] and *Li et al.* [2010]. The large increase in OH is not only the direct result of photolysis of additional HONO, but it is also due to the OH production from the photolysis of additional secondary VOCs from the oxidation of primary VOCs by additional OH [*Aumont et al.*, 2003]. The enhancements in OH lead to more production of O_3 especially during noontime, with the largest O_3 increases during 10:00-12:00 LTC, as shown in Figure 10a. The maximum hourly ozone enhancement reached 27.4 ppb on 27 August with the mean ozone concentration increased by 8.2% over the whole simulation period at the TC site.

Overall, the simulated O_3 concentrations were in very good agreement with the observations at different monitoring stations across Hong Kong although the model underestimated at noontime at urban and suburban sites such as Central and TC (Figure 11). Compared with the BASE case, the LOAES case had noticeable enhancements in simulated O_3 especially during noontime at these sites. The additional sources of HONO initiated the O_3 production 1-2 hours earlier in the morning at most of the stations, similar to the findings in *Lei et al.* [2004] and *Li et al.* [2010]. After 14:00, as HONO no longer promoted the production of OH, the additional O_3 production in the LOAES case became negligible (Figure 11).

The inclusion of HONO sources have improved the WRF-Chem simulations of both daily and peak O_3 concentrations during noontime at multiple stations over Hong Kong. As shown in Table 5, the mean biases between the simulated and observed values of 8-hour and 1-hour maxima O_3 in the LOAES case have appreciable improvements, decreasing from -10.03 ppb in the BASE case to -0.53 ppb and from -21.77 ppb in the BASE case to -9.17 ppb, respectively. The daily average O_3 concentration at the measurement stations also increased from 30.34 ppb in the BASE case to 31.99 ppb in the LOAES case, much closer to the actual observations.

3.4.2. Enhancements in regional ozone levels over the HK-PRD region

Figure 12 presents the distribution of modeled O_3 at 14:00 LTC in the BASE and LOAES cases over the PRD region for the episode period. As shown, high levels of O_3 of up to 80-100 ppb occurred over the northern parts of the PRD. As evidenced, higher O_3 concentrations were shown over the downwind areas of the PRD in the LOAES case, especially over Hong Kong (Figure 12c and f). We also separately examined the impact of the source from ocean surface and from soil bacterial emissions. The results show that the oceanic HONO had unneglectable impacts on O_3 concentrations (0.2-1.0 ppb) over the PRD and the coastal areas of Yangtze River Delta region (Figure S4b) and that the HONO from soil bacteria enhanced O_3 levels by 0.5-2.0 ppb over the PRD region (Figure S5b).

We next examine O_3 enhancements in the LOAES case in different urban areas of the PRD region. The urban areas were identified based on MODIS land-use data. As shown in Table 6, compared with the BASE case, increases in O_3 at 14:00 LTC in the LOAES case were up to 12 ppb in urban Hong Kong (Figure 12f) with an average of 7.7 ppb. The O_3 changes in other major cities of the PRD were also noticeable as shown in Table 6. Over urban Guangzhou (GZ) and Shenzhen (SZ), where abundant anthropogenic emissions exist, the respective increases in daily O_3 level reached nearly 12% (4.1 ppb) and 10% (3.2 ppb) on average. In Huizhou (HZ), which is less industrialized, the daily ozone enhancement also reached nearly 6%. These results indicate the considerable contribution of the additional HONO sources to O_3 formation in the urban areas of the whole PRD region.

4. Summary and conclusions

In this study, comprehensive HONO sources were incorporated into the WRF-Chem model and the revised model showed significant improvements in the simulation of atmospheric HONO concentrations observed at a suburban site that is surrounded by complex land coverages. Although the well-recognized heterogeneous conversions of NO_2 on the ground surface made the largest contribution to the observed HONO, soil biological activities and oceanic sources, with contributions of ~29% and ~9%, respectively, were also shown to be important at the suburban site. Our modeling results suggest that the soil biological activities and/or oceanic source could contribute substantial fractions of HONO in the atmosphere and there is a need to consider these two new sources over specific regions: in the areas covered with abundant natural or artificial vegetation (such as cotton and wheat fields that are abundant in China and have large emission fluxes of HONO [*Oswald et al.*, 2013]) and/or areas adjacent to ocean (such as coastal areas along the eastern China that are home to most of this country's megacities such as Tianjin, Shanghai, and Guangzhou). The incorporation of the additional HONO sources has appreciably improved the predictions of ozone at multiple monitoring stations and led to a 6-12% enhancement in averaged ozone over the urban areas of the HK-PRD region. Our study highlights the need to include these sources into regional air quality models before using the models to refine ozone control polices.

Acknowledgements. The authors would like to thank the China Meteorological Administration for providing the meteorological observations and the Hong Kong Environmental Protection Department for the O_3 observations and emission inventory over Hong Kong. The numerical calculations in this paper have been done on the IBM Blade cluster system in the High Performance Computing Center (HPCC) of Nanjing University and the HPC at PolyU. This work was supported by the Hong Kong PhD Fellowship Scheme, PolyU Project of Strategic Importance (1-ZE13) and Collaborative Research Fund of the Hong Kong Research Grants Council (C5022-14G). Both the data and source codes of the revised WRF-Chem model used in this study are available from the authors upon request (cetwang@polyu.edu.hk).

References

Alicke, B., A. Geyer, A. Hofzumahaus, F. Holland, S. Konrad, H. W. Pätz, J. Schäfer, J. Stutz, A. Volz-Thomas, and U. Platt (2003), OH formation by HONO photolysis during the BERLIOZ experiment, *Journal of Geophysical Research: Atmospheres*, *108*(D4), 8247, doi:10.1029/2001JD000579.

Ammann, M., E. Rössler, R. Strekowski, and C. George (2005), Nitrogen dioxide multiphase chemistry: Uptake kinetics on aqueous solutions containing phenolic compounds, *Physical Chemistry Chemical Physics*, *7*(12), 2513-2518.

An, J., Y. Li, Y. Chen, J. Li, Y. Qu, and Y. Tang (2013), Enhancements of major aerosol components due to additional HONO sources in the North China Plain and implications for visibility and haze, *Adv. Atmos. Sci.*, *30*(1), 57-66, doi:10.1007/s00376-012-2016-9.

An, J., Y. Li, F. Wang, and P. Xie (2011), *Impacts of Photoexcited NO2 Chemistry and Heterogeneous Reactions on Concentrations of O3 and NOy in Beijing,Tianjin and Hebei Province of China*, doi:16154.

Aumont, B., F. Chervier, and S. Laval (2003), Contribution of HONO sources to the NOx/HOx/O3 chemistry in the polluted boundary layer, *Atmospheric Environment*, *37*(4), 487-498, doi:http://dx.doi.org/10.1016/S1352-2310(02)00920-2.

Bejan, I., Y. Abd El Aal, I. Barnes, T. Benter, B. Bohn, P. Wiesen, and J. Kleffmann (2006), The photolysis of ortho-nitrophenols: a new gas phase source of HONO, *Physical Chemistry Chemical Physics*, *8*(17), 2028-2035, doi:10.1039/B516590C.

Chen, F., and J. Dudhia (2001), Coupling an Advanced Land Surface–Hydrology Model with the Penn State–NCAR MM5 Modeling System. Part I: Model Implementation and Sensitivity, *Monthly Weather Review*, *129*(4), 569-585, doi:10.1175/1520-0493(2001)129<0569:CAALSH>2.0.CO;2.

Chou, M.-D., M. J. Suarez, C.-H. Ho, M. M. H. Yan, and K.-T. Lee (1998), Parameterizations for Cloud Overlapping and Shortwave Single-Scattering Properties for Use in General Circulation and Cloud Ensemble Models, *Journal of Climate*, *11*(2), 202-214, doi:10.1175/1520-0442(1998)011<0202:PFCOAS>2.0.CO;2.

Colussi, A. J., S. Enami, A. Yabushita, M. R. Hoffmann, W.-G. Liu, H. Mishra, and I. I. I. W. A. Goddard (2013), Tropospheric aerosol as a reactive intermediate, *Faraday Discussions*, *165*(0), 407-420, doi:10.1039/C3FD00040K.

Czader, B. H., Y. Choi, X. Li, S. Alvarez, and B. Lefer (2015), Impact of updated traffic emissions on HONO mixing ratios simulated for urban site in Houston, Texas, *Atmos. Chem. Phys.*, *15*(3), 1253-1263, doi:10.5194/acp-15-1253-2015.

Czader, B. H., B. Rappenglück, P. Percell, D. W. Byun, F. Ngan, and S. Kim (2012), Modeling nitrous acid and its impact on ozone and hydroxyl radical during the Texas Air Quality Study 2006, *Atmos. Chem. Phys.*, *12*(15), 6939-6951, doi:10.5194/acp-12-6939-2012.

Ding, A., T. Wang, M. Zhao, T. Wang, and Z. Li (2004), Simulation of sea-land breezes and a discussion of their implications on the transport of air pollution during a multi-day ozone episode in the Pearl River Delta of China, *Atmospheric Environment*, *38*(39), 6737-6750, doi:http://dx.doi.org/10.1016/j.atmosenv.2004.09.017.

Donaldson, M. A., A. E. Berke, and J. D. Raff (2013), Uptake of Gas Phase Nitrous Acid onto Boundary Layer Soil Surfaces, *Environmental Science & Technology*, *48*(1), 375-383, doi:10.1021/es404156a.

Elshorbany, Y. F., B. Steil, C. Brühl, and J. Lelieveld (2012), Impact of HONO on global atmospheric chemistry calculated with an empirical parameterization in the EMAC model, *Atmos. Chem. Phys.*, *12*(20), 9977-10000, doi:10.5194/acp-12-9977-2012.

Emmons, L. K., et al. (2010), Description and evaluation of the Model for Ozone and Related chemical Tracers, version 4 (MOZART-4), *Geosci. Model Dev.*, *3*(1), 43-67, doi:10.5194/gmd-3-43-2010.

Fahey, K. M., and S. N. Pandis (2001), Optimizing model performance: variable size resolution in cloud chemistry modeling, *Atmospheric Environment*, *35*(26), 4471-4478, doi:http://dx.doi.org/10.1016/S1352-2310(01)00224-2.

Fast, J. D., W. I. Gustafson, R. C. Easter, R. A. Zaveri, J. C. Barnard, E. G. Chapman, G. A. Grell, and S. E. Peckham (2006), Evolution of ozone, particulates, and aerosol direct radiative forcing in the vicinity of Houston using a fully coupled meteorology-chemistry-aerosol model, *Journal of Geophysical Research: Atmospheres*, *111*(D21), D21305, doi:10.1029/2005JD006721.

Foley, K., S. Roselle, K. Appel, P. Bhave, J. Pleim, T. Otte, R. Mathur, G. Sarwar, J. Young, and R. Gilliam (2009), Incremental testing of the Community Multiscale Air Quality (CMAQ) modeling system version 4.7, *Geoscientific Model Development Discussions*, *2*(2), 1245-1297.

Gao, J., T. Wang, X. Zhou, W. Wu, and W. Wang (2009), Measurement of aerosol number size distributions in the Yangtze River delta in China: Formation and growth of particles under polluted conditions, *Atmospheric Environment*, *43*(4), 829-836, doi:http://dx.doi.org/10.1016/j.atmosenv.2008.10.046.

George, C., R. S. Strekowski, J. Kleffmann, K. Stemmler, and M. Ammann (2005), Photoenhanced uptake of gaseous NO2 on solid organic compounds: a photochemical source of HONO?, *Faraday Discussions*, *130*(0), 195-210, doi:10.1039/B417888M.

Gonçalves, M., D. Dabdub, W. L. Chang, O. Jorba, and J. M. Baldasano (2012), Impact of HONO sources on the performance of mesoscale air quality models, *Atmospheric Environment*, *54*(0), 168-176, doi:http://dx.doi.org/10.1016/j.atmosenv.2012.02.079.

Grell, G. A., and D. Dévényi (2002), A generalized approach to parameterizing convection combining ensemble and data assimilation techniques, *Geophys. Res. Lett.*, *29*(14), 38-31-38-34, doi:10.1029/2002GL015311.

Grell, G. A., S. E. Peckham, R. Schmitz, S. A. McKeen, G. Frost, W. C. Skamarock, and B. Eder (2005), Fully coupled “online” chemistry within the WRF model, *Atmos. Environ.*, *39*(37), 6957-6975, doi:http://dx.doi.org/10.1016/j.atmosenv.2005.04.027.

Guenther, A., T. Karl, P. Harley, C. Wiedinmyer, P. I. Palmer, and C. Geron (2006), Estimates of global terrestrial isoprene emissions using MEGAN (Model of Emissions of Gases and Aerosols from Nature), *Atmos. Chem. Phys.*, *6*(11), 3181-3210, doi:10.5194/acp-6-3181-2006.

Gutzwiller, L., F. Arens, U. Baltensperger, H. W. Gäggeler, and M. Ammann (2002), Significance of Semivolatile Diesel Exhaust Organics for Secondary HONO Formation, *Environmental Science & Technology*, *36*(4), 677-682, doi:10.1021/es015673b.

He, Y., X. Zhou, J. Hou, H. Gao, and S. B. Bertman (2006), Importance of dew in controlling the air-surface exchange of HONO in rural forested environments, *Geophysical Research Letters*, *33*(2), L02813, doi:10.1029/2005GL024348.

Heland, J., J. Kleffmann, R. Kurtenbach, and P. Wiesen (2001), A New Instrument To Measure Gaseous Nitrous Acid (HONO) in the Atmosphere, *Environmental Science & Technology*, *35*(15), 3207-3212, doi:10.1021/es000303t.

Hong, S.-Y., Y. Noh, and J. Dudhia (2006), A New Vertical Diffusion Package with an Explicit Treatment of Entrainment Processes, *Monthly Weather Review*, *134*(9), 2318-2341, doi:10.1175/MWR3199.1.

Huber, J. R. (2004), Photochemistry of Molecules Relevant to the Atmosphere: Photodissociation of Nitric Acid in the Gas Phase, *ChemPhysChem*, *5*(11), 1663-1669, doi:10.1002/cphc.200400071.

Kirchstetter, T. W., R. A. Harley, and D. Littlejohn (1996), Measurement of Nitrous Acid in Motor Vehicle Exhaust, *Environmental Science & Technology*, *30*(9), 2843-2849, doi:10.1021/es960135y.

Kleffmann, J. (2007), Daytime Sources of Nitrous Acid (HONO) in the Atmospheric Boundary Layer, *ChemPhysChem*, *8*(8), 1137-1144, doi:10.1002/cphc.200700016.

Kleffmann, J., K. H. Becker, and P. Wiesen (1998), Heterogeneous NO2 conversion processes on acid surfaces: possible atmospheric implications, *Atmospheric Environment*, *32*(16), 2721-2729, doi:http://dx.doi.org/10.1016/S1352-2310(98)00065-X.

Kleffmann, J., T. Gavriloaiei, A. Hofzumahaus, F. Holland, R. Koppmann, L. Rupp, E. Schlosser, M. Siese, and A. Wahner (2005), Daytime formation of nitrous acid: A major source of OH radicals in a forest, *Geophysical Research Letters*, *32*(5), L05818, doi:10.1029/2005GL022524.

Kleffmann, J., R. Kurtenbach, J. Lörzer, P. Wiesen, N. Kalthoff, B. Vogel, and H. Vogel (2003), Measured and simulated vertical profiles of nitrous acid—Part I: Field measurements, *Atmospheric Environment*, *37*(21), 2949-2955, doi:http://dx.doi.org/10.1016/S1352-2310(03)00242-5.

Kleffmann, J., and P. Wiesen (2008), Technical Note: Quantification of interferences of wet chemical HONO LOPAP measurements under simulated polar conditions, *Atmos. Chem. Phys.*, *8*(22), 6813-6822, doi:10.5194/acp-8-6813-2008.

Kurtenbach, R., K. H. Becker, J. A. G. Gomes, J. Kleffmann, J. C. Lörzer, M. Spittler, P. Wiesen, R. Ackermann, A. Geyer, and U. Platt (2001), Investigations of emissions and heterogeneous formation of HONO in a road traffic tunnel, *Atmospheric Environment*, *35*(20), 3385-3394, doi:http://dx.doi.org/10.1016/S1352-2310(01)00138-8.

Kusaka, H., H. Kondo, Y. Kikegawa, and F. Kimura (2001), A Simple Single-Layer Urban Canopy Model For Atmospheric Models: Comparison With Multi-Layer And Slab Models, *Boundary-Layer Meteorology*, *101*(3), 329-358, doi:10.1023/A:1019207923078.

Lam, K. S., T. J. Wang, C. L. Wu, and Y. S. Li (2005), Study on an ozone episode in hot season in Hong Kong and transboundary air pollution over Pearl River Delta region of China, *Atmospheric Environment*, *39*(11), 1967-1977, doi:http://dx.doi.org/10.1016/j.atmosenv.2004.11.023.

Lei, W., R. Zhang, X. Tie, and P. Hess (2004), Chemical characterization of ozone formation in the Houston-Galveston area: A chemical transport model study, *Journal of Geophysical Research: Atmospheres*, *109*(D12), D12301, doi:10.1029/2003JD004219.

Lei, Y., Q. Zhang, K. B. He, and D. G. Streets (2011), Primary anthropogenic aerosol emission trends for China, 1990–2005, *Atmos. Chem. Phys.*, *11*(3), 931-954, doi:10.5194/acp-11-931-2011.

Li, G., W. Lei, M. Zavala, R. Volkamer, S. Dusanter, P. Stevens, and L. T. Molina (2010), Impacts of HONO sources on the photochemistry in Mexico City during the MCMA-2006/MILAGO Campaign, *Atmos. Chem. Phys.*, *10*(14), 6551-6567, doi:10.5194/acp-10-6551-2010.

Li, M., et al. (2014a), Mapping Asian anthropogenic emissions of non-methane volatile organic compounds to multiple chemical mechanisms, *Atmos. Chem. Phys.*, *14*(11), 5617-5638, doi:10.5194/acp-14-5617-2014.

Li, S., J. Matthews, and A. Sinha (2008), Atmospheric Hydroxyl Radical Production from Electronically Excited NO2 and H2O, *Science*, *319*(5870), 1657-1660, doi:10.1126/science.1151443.

Li, X., et al. (2012), Exploring the atmospheric chemistry of nitrous acid (HONO) at a rural site in Southern China, *Atmos. Chem. Phys.*, *12*(3), 1497-1513, doi:10.5194/acp-12-1497-2012.

Li, X., et al. (2014b), Missing Gas-Phase Source of HONO Inferred from Zeppelin Measurements in the Troposphere, *Science*, *344*(6181), 292-296, doi:10.1126/science.1248999.

Li, X., et al. (2015), Response to Comment on "Missing gas-phase source of HONO inferred from Zeppelin measurements in the troposphere", *Science*, *348*(6241), 1326, doi:10.1126/science.aaa3777.

Li, Y., J. An, M. Min, W. Zhang, F. Wang, and P. Xie (2011), Impacts of HONO sources on the air quality in Beijing, Tianjin and Hebei Province of China, *Atmospheric Environment*, *45*(27), 4735-4744, doi:http://dx.doi.org/10.1016/j.atmosenv.2011.04.086.

Lin, Y.-L., R. D. Farley, and H. D. Orville (1983), Bulk Parameterization of the Snow Field in a Cloud Model, *Journal of Climate and Applied Meteorology*, *22*(6), 1065-1092, doi:10.1175/1520-0450(1983)022<1065:BPOTSF>2.0.CO;2.

Liu, Z., et al. (2012), Summertime photochemistry during CAREBeijing-2007: ROx budgets and O3 formation, *Atmos. Chem. Phys.*, *12*(16), 7737-7752, doi:10.5194/acp-12-7737-2012.

Maljanen, M., P. Yli-Pirilä, J. Hytönen, J. Joutsensaari, and P. J. Martikainen (2013), Acidic northern soils as sources of atmospheric nitrous acid (HONO), *Soil Biology and Biochemistry*, *67*(0), 94-97, doi:http://dx.doi.org/10.1016/j.soilbio.2013.08.013.

Michoud, V., et al. (2013), Study of the unknown HONO daytime source at an European suburban site during the MEGAPOLI summer and winter field campaigns, *Atmos. Chem. Phys. Discuss.*, *13*(9), 23639-23690, doi:10.5194/acpd-13-23639-2013.

Mlawer, E. J., S. J. Taubman, P. D. Brown, M. J. Iacono, and S. A. Clough (1997), Radiative transfer for inhomogeneous atmospheres: RRTM, a validated correlated-k model for the longwave, *Journal of Geophysical Research: Atmospheres*, *102*(D14), 16663-16682, doi:10.1029/97JD00237.

Monge, M. E., B. D'Anna, L. Mazri, A. Giroir-Fendler, M. Ammann, D. J. Donaldson, and C. George (2010), Light changes the atmospheric reactivity of soot, *Proceedings of the National Academy of Sciences*, *107*(15), 6605-6609, doi:10.1073/pnas.0908341107.

Ndour, M., B. D'Anna, C. George, O. Ka, Y. Balkanski, J. Kleffmann, K. Stemmler, and M. Ammann (2008), Photoenhanced uptake of NO2 on mineral dust: Laboratory experiments and model simulations, *Geophysical Research Letters*, *35*(5), L05812, doi:10.1029/2007GL032006.

Oswald, R., et al. (2013), HONO Emissions from Soil Bacteria as a Major Source of Atmospheric Reactive Nitrogen, *Science*, *341*(6151), 1233-1235, doi:10.1126/science.1242266.

Rappenglück, B., G. Lubertino, S. Alvarez, J. Golovko, B. Czader, and L. Ackermann (2013), Radical precursors and related species from traffic as observed and modeled at an urban highway junction, *Journal of the Air & Waste Management Association*, *63*(11), 1270-1286.

Rubio, M. A., E. Lissi, and G. Villena (2008), Factors determining the concentration of nitrite in dew from Santiago, Chile, *Atmospheric Environment*, *42*(33), 7651-7656, doi:http://dx.doi.org/10.1016/j.atmosenv.2008.05.055.

Rubio, M. A., E. Lissi, G. Villena, Y. F. Elshorbany, J. Kleffmann, R. Kurtenbach, and P. Wiesen (2009), Simultaneous measurements of formaldehyde and nitrous acid in dews and gas phase in the atmosphere of Santiago, Chile, *Atmospheric Environment*, *43*(38), 6106-6109, doi:http://dx.doi.org/10.1016/j.atmosenv.2009.09.017.

Sarwar, G., S. J. Roselle, R. Mathur, W. Appel, R. L. Dennis, and B. Vogel (2008), A comparison of CMAQ HONO predictions with observations from the Northeast Oxidant and Particle Study, *Atmospheric Environment*, *42*(23), 5760-5770, doi:http://dx.doi.org/10.1016/j.atmosenv.2007.12.065.

Stemmler, K., M. Ammann, C. Donders, J. Kleffmann, and C. George (2006), Photosensitized reduction of nitrogen dioxide on humic acid as a source of nitrous acid, *Nature*, *440*(7081), 195-198, doi:http://www.nature.com/nature/journal/v440/n7081/suppinfo/nature04603_S1.html.

Su, H., Y. Cheng, R. Oswald, T. Behrendt, I. Trebs, F. X. Meixner, M. O. Andreae, P. Cheng, Y. Zhang, and U. Pöschl (2011), Soil Nitrite as a Source of Atmospheric HONO and OH Radicals, *Science*, *333*(6049), 1616-1618, doi:10.1126/science.1207687.

Svensson, R., E. Ljungström, and O. Lindqvist (1987), Kinetics of the reaction between nitrogen dioxide and water vapour, *Atmospheric Environment (1967)*, *21*(7), 1529-1539, doi:http://dx.doi.org/10.1016/0004-6981(87)90315-5.

Tyndall, G. S., J. J. Orlando, and J. G. Calvert (1995), Upper Limit for the Rate Coefficient for the Reaction HO2 + NO2 .fwdarw. HONO + O2, *Environmental Science & Technology*, *29*(1), 202-206, doi:10.1021/es00001a026.

VandenBoer, T. C., et al. (2013), Understanding the role of the ground surface in HONO vertical structure: High resolution vertical profiles during NACHTT-11, *Journal of Geophysical Research: Atmospheres*, *118*(17), 10,155-110,171, doi:10.1002/jgrd.50721.

VandenBoer, T. C., et al. (2014), Evidence for a nitrous acid (HONO) reservoir at the ground surface in Bakersfield, CA, during CalNex 2010, *Journal of Geophysical Research: Atmospheres*, 2013JD020971, doi:10.1002/2013JD020971.

Vogel, B., H. Vogel, J. Kleffmann, and R. Kurtenbach (2003), Measured and simulated vertical profiles of nitrous acid—Part II. Model simulations and indications for a photolytic source, *Atmospheric Environment*, *37*(21), 2957-2966, doi:http://dx.doi.org/10.1016/S1352-2310(03)00243-7.

Volkamer, R., P. Sheehy, L. T. Molina, and M. J. Molina (2010), Oxidative capacity of the Mexico City atmosphere – Part 1: A radical source perspective, *Atmos. Chem. Phys.*, *10*(14), 6969-6991, doi:10.5194/acp-10-6969-2010.

Wong, K. W., H. J. Oh, B. L. Lefer, B. Rappenglück, and J. Stutz (2011), Vertical profiles of nitrous acid in the nocturnal urban atmosphere of Houston, TX, *Atmos. Chem. Phys.*, *11*(8), 3595-3609, doi:10.5194/acp-11-3595-2011.

Wong, K. W., C. Tsai, B. Lefer, N. Grossberg, and J. Stutz (2013), Modeling of daytime HONO vertical gradients during SHARP 2009, *Atmos. Chem. Phys.*, *13*(7), 3587-3601, doi:10.5194/acp-13-3587-2013.

Xu, Z., T. Wang, J. Wu, L. Xue, J. Chan, Q. Zha, S. Zhou, P. K. K. Louie, and C. W. Y. Luk (2015), Nitrous acid (HONO) in a polluted subtropical atmosphere: Seasonal variability, direct vehicle emissions and heterogeneous production at ground surface, *Atmospheric Environment*, *106*(0), 100-109, doi:http://dx.doi.org/10.1016/j.atmosenv.2015.01.061.

Yabushita, A., S. Enami, Y. Sakamoto, M. Kawasaki, M. R. Hoffmann, and A. J. Colussi (2009), Anion-Catalyzed Dissolution of NO2 on Aqueous Microdroplets, *The Journal of Physical Chemistry A*, *113*(17), 4844-4848, doi:10.1021/jp900685f.

Ye, C., X. Zhou, D. Pu, J. Stutz, J. Festa, M. Spolaor, C. Cantrell, R. L. Mauldin, A. Weinheimer, and J. Haggerty (2015), Comment on "Missing gas-phase source of HONO inferred from Zeppelin measurements in the troposphere", *Science*, *348*(6241), 1326, doi:10.1126/science.aaa1992.

Zaveri, R. A., R. C. Easter, J. D. Fast, and L. K. Peters (2008), Model for Simulating Aerosol Interactions and Chemistry (MOSAIC), *Journal of Geophysical Research: Atmospheres*, *113*(D13), D13204, doi:10.1029/2007JD008782.

Zaveri, R. A., and L. K. Peters (1999), A new lumped structure photochemical mechanism for large-scale applications, *Journal of Geophysical Research: Atmospheres*, *104*(D23), 30387-30415, doi:10.1029/1999JD900876.

Zha, Q., L. Xue, T. Wang, Z. Xu, C. Yeung, P. K. K. Louie, and C. W. Y. Luk (2014), Large conversion rates of NO2 to HNO2 observed in air masses from the South China Sea: Evidence of strong production at sea surface?, *Geophysical Research Letters*, *41*(21), 2014GL061429, doi:10.1002/2014GL061429.

Zhang, L., T. Wang, M. Lv, and Q. Zhang (2015), On the severe haze in Beijing during January 2013: Unraveling the effects of meteorological anomalies with WRF-Chem, *Atmospheric Environment*, *104*(0), 11-21, doi:http://dx.doi.org/10.1016/j.atmosenv.2015.01.001.

Zhang, N., X. Zhou, P. B. Shepson, H. Gao, M. Alaghmand, and B. Stirm (2009a), Aircraft measurement of HONO vertical profiles over a forested region, *Geophysical Research Letters*, *36*(15), L15820, doi:10.1029/2009GL038999.

Zhang, Q., et al. (2009b), Asian emissions in 2006 for the NASA INTEX-B mission, *Atmos. Chem. Phys.*, *9*(14), 5131-5153, doi:10.5194/acp-9-5131-2009.

Zhang, R., G. Sarwar, J. C. H. Fung, A. K. H. Lau, and Y. Zhang (2012), Examining the Impact of Nitrous Acid Chemistry on Ozone and PM over the Pearl River Delta Region, *Advances in Meteorology*, *2012*, 18, doi:10.1155/2012/140932.

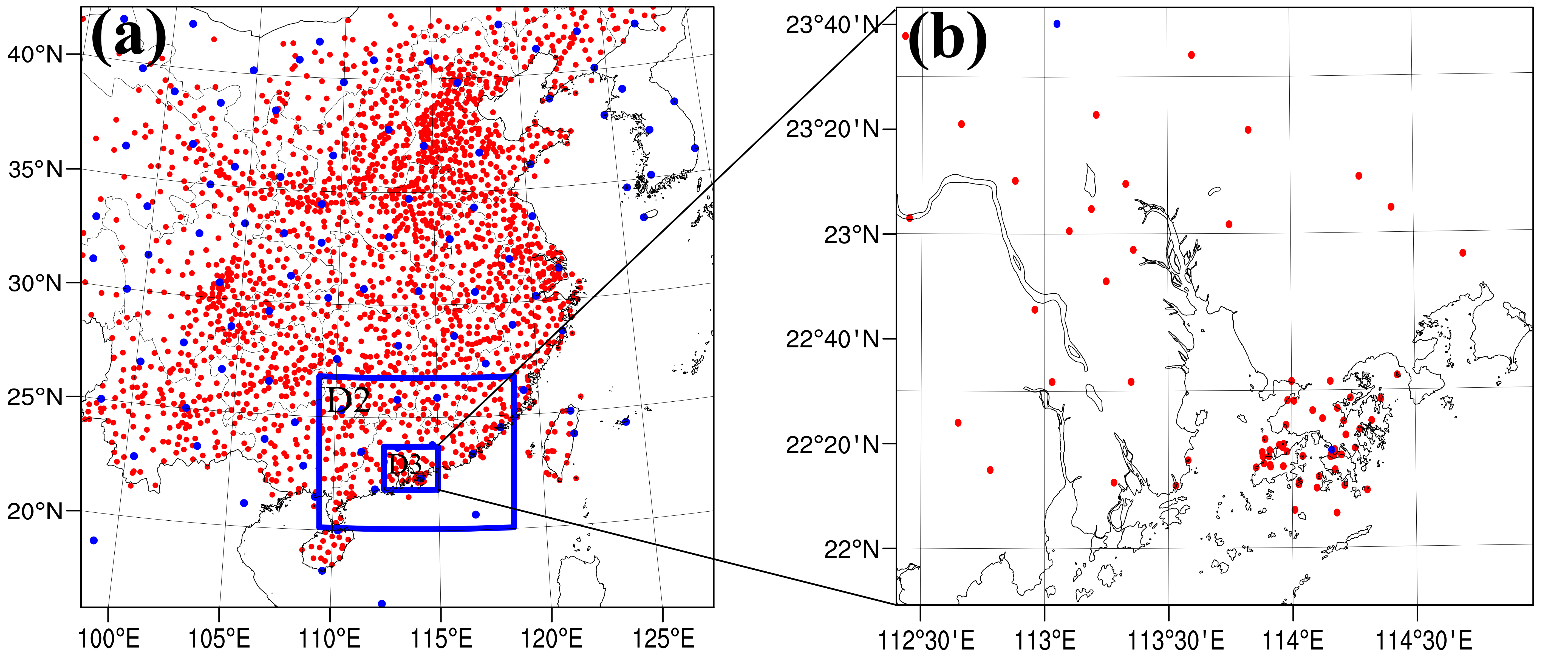
(a)
40°N
35°N
30°N
25°N
20°N
100°E
105°E
110°E
115°E
120°E
125°E
D2
D3
(b)
23°40'N
23°20'N
23°N
22°40'N
22°20'N
22°N
112°30'E
113°E
113°30'E
114°E
114°30'E

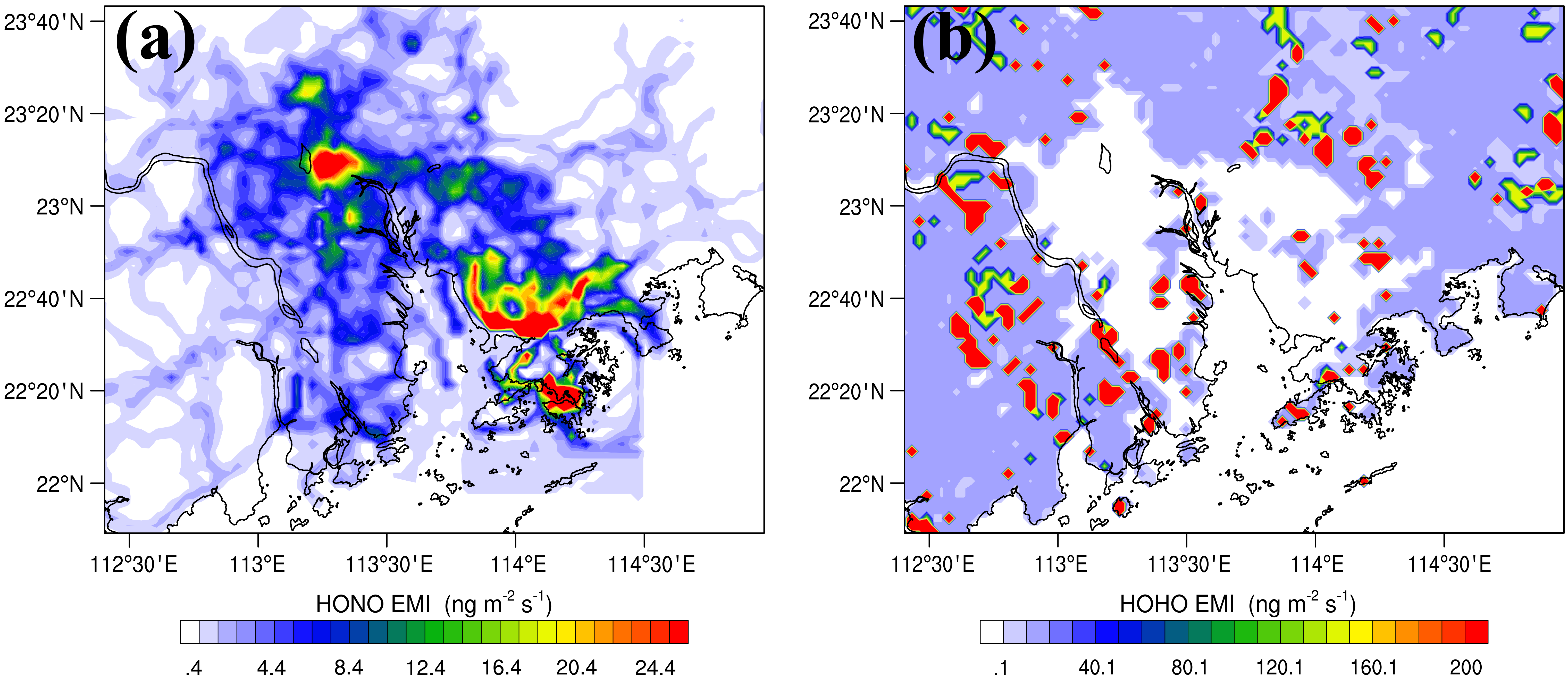

(a)
23°40'N
23°20'N
23°N
22°40'N
22°20'N
22°N
112°30'E
113°E
113°30'E
114°E
114°30'E
HONO EMI (ng m-2 s-1)
.4
4.4
8.4
12.4
16.4
20.4
24.4
(b)
23°40'N
23°20'N
23°N
22°40'N
22°20'N
22°N
112°30'E
113°E
113°30'E
114°E
114°30'E
HOHO EMI (ng m-2 s-1)
.1
40.1
80.1
120.1
160.1
200


TAP MUN
YUEN LONG
TAI PO
SHATIN
TSUEN WAN
KWAI CHUNG
SHAM SHUI PO
KWUN TONG
CENTRAL
WESTERN
EASTERN
TUNG CHUNG
HOK TSUI
N
10 km

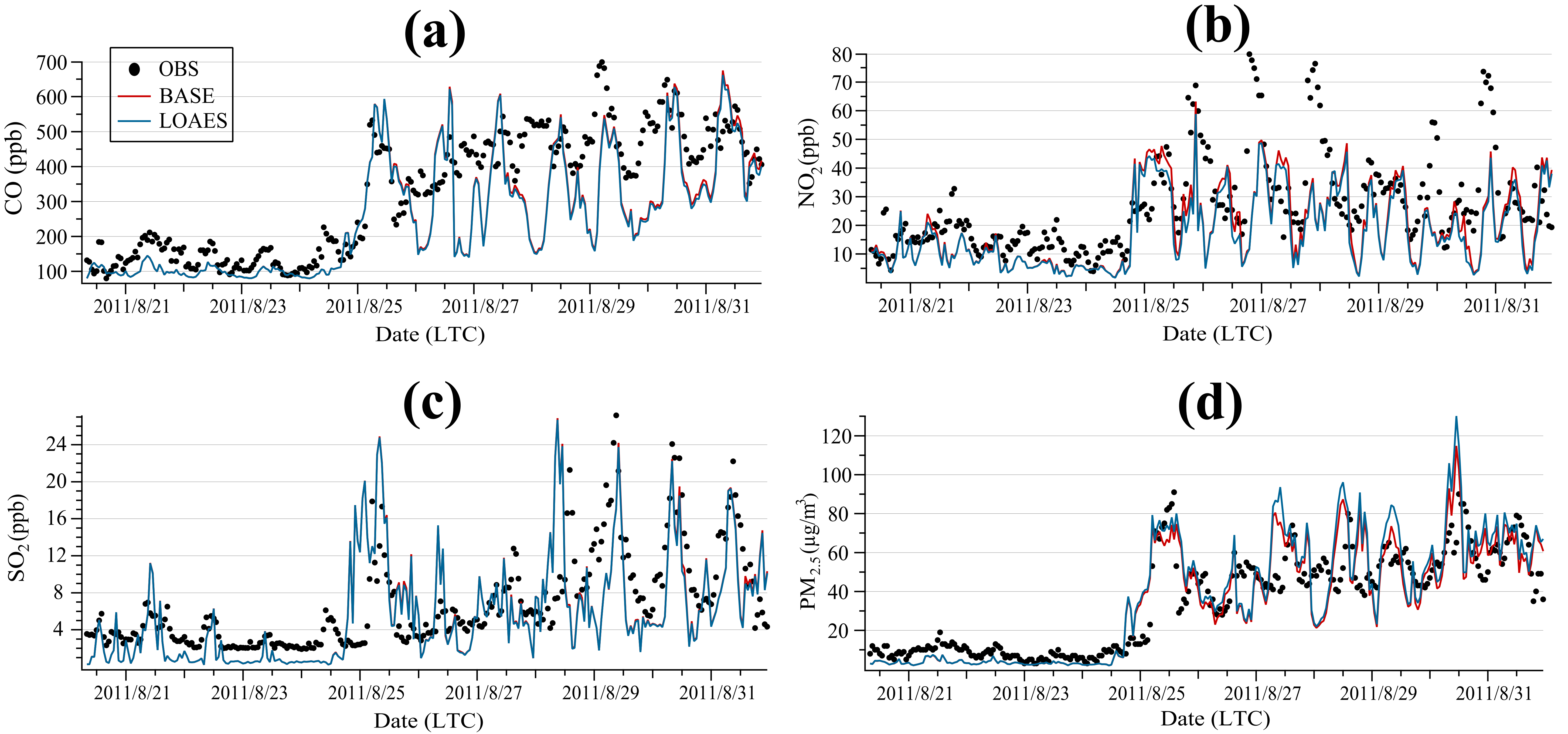

(a)
(b)
(c)
(d)
OBS
BASE
LOAES
CO (ppb)
NO2 (ppb)
SO2 (ppb)
PM2.5 (μg/m3)
2011/8/21
2011/8/23
2011/8/25
2011/8/27
2011/8/29
2011/8/31
Date (LTC)

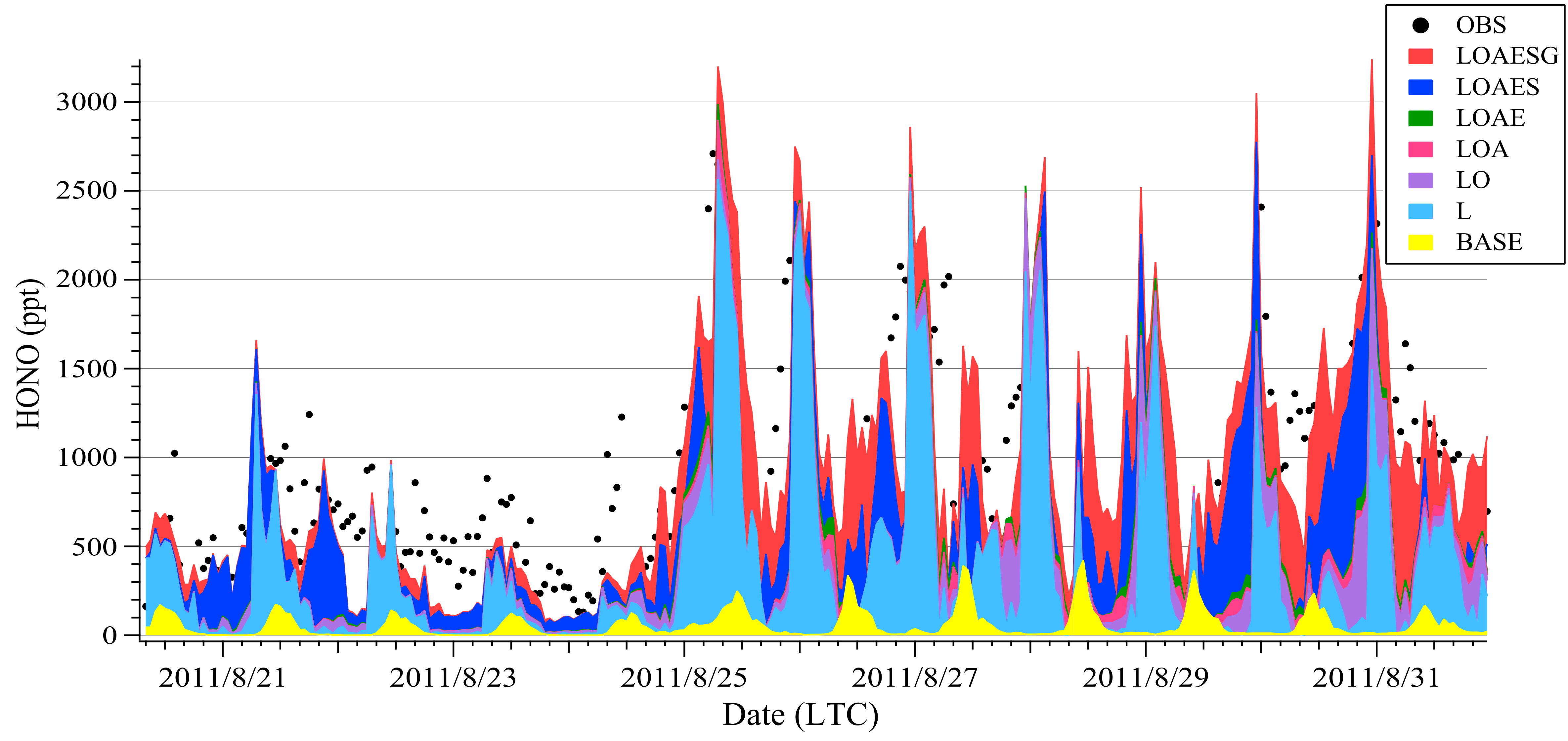

HONO (ppt)
3000
2500
2000
1500
1000
500
0
2011/8/21
2011/8/23
2011/8/25
2011/8/27
2011/8/29
2011/8/31
Date (LTC)
OBS
LOAESG
LOAES
LOAE
LOA
LO
L
BASE

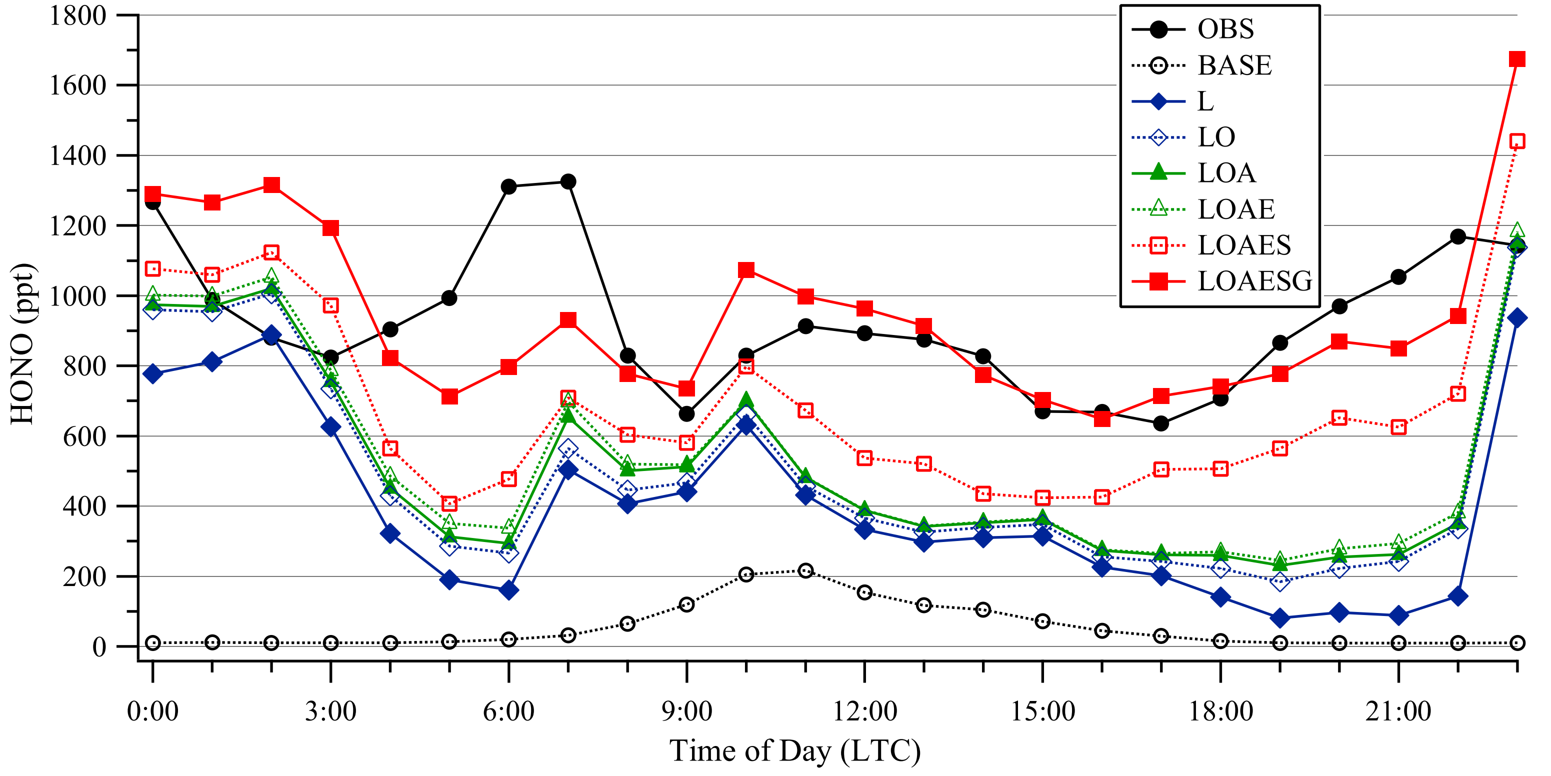

OBS
BASE
L
LO
LOA
LOAE
LOAES
LOAESG
HONO (ppt)
0
200
400
600
800
1000
1200
1400
1600
1800
0:00
3:00
6:00
9:00
12:00
15:00
18:00
21:00
Time of Day (LTC)

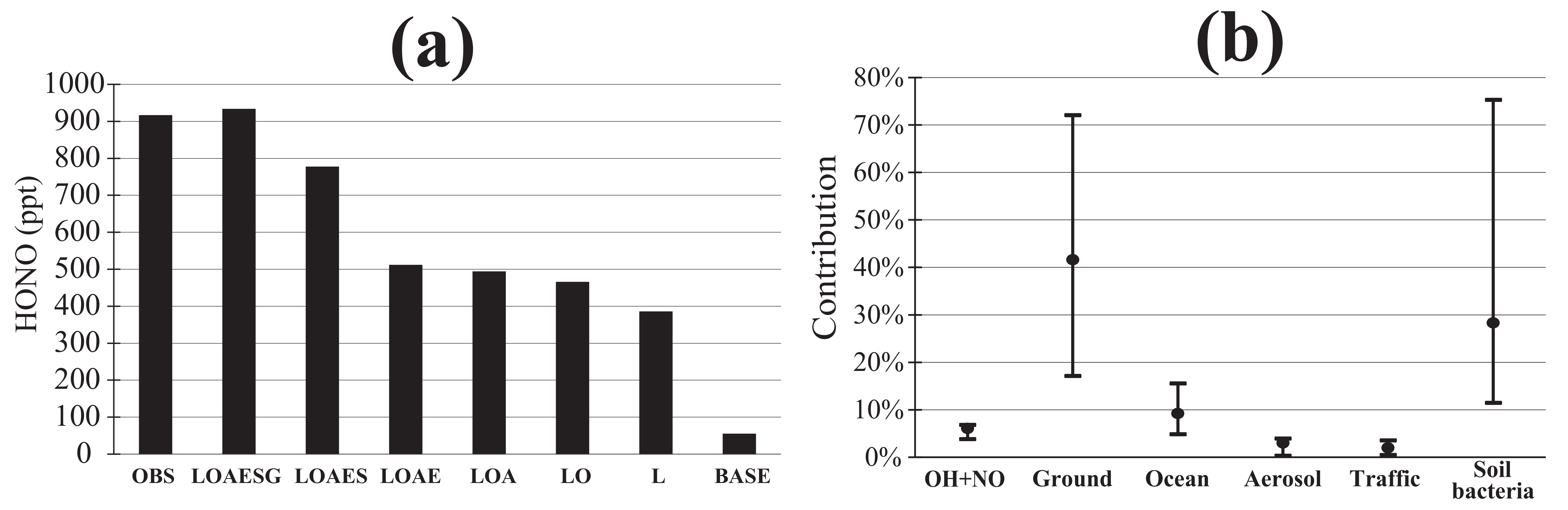
(a)
HONO (ppt)
1000
900
800
700
600
500
400
300
200
100
0
OBS
LOAESG
LOAES
LOAE
LOA
LO
L
BASE
(b)
Contribution
80%
70%
60%
50%
40%
30%
20%
10%
0%
OH+NO
Ground
Ocean
Aerosol
Traffic
Soil
bacteria

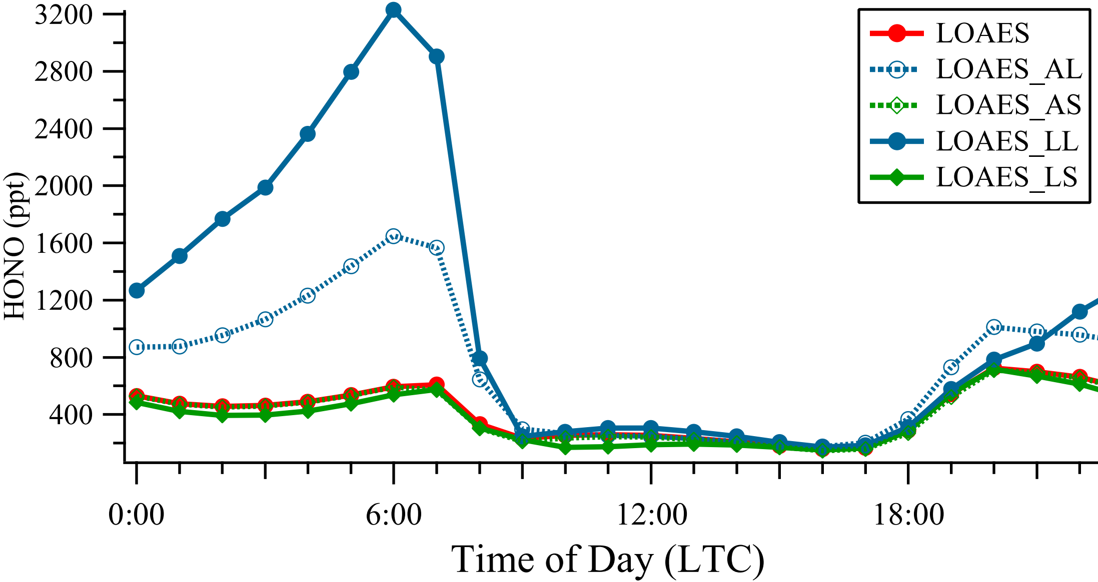

LOAES
LOAES_AL
LOAES_AS
LOAES_LL
LOAES_LS
HONO (ppt)
3200
2800
2400
2000
1600
1200
800
400
0:00
6:00
12:00
18:00
Time of Day (LTC)

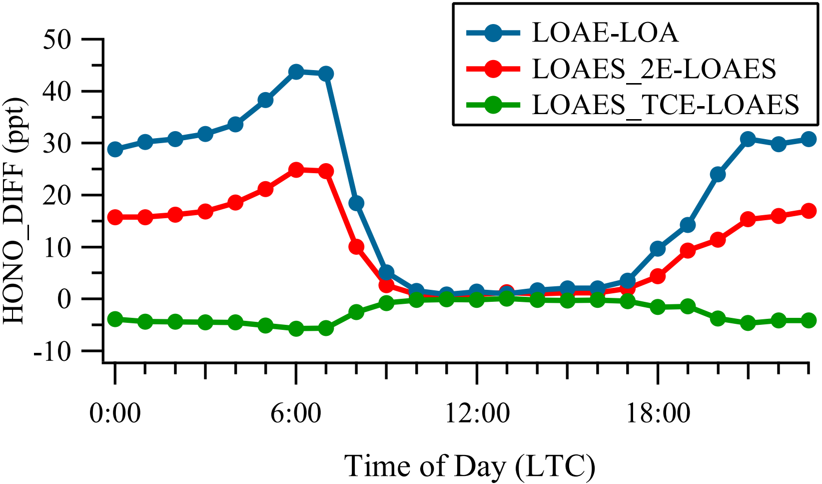

LOAE-LOA
LOAES_2E-LOAES
LOAES_TCE-LOAES
50
40
30
20
10
0
-10
HONO_DIFF (ppt)
0:00
6:00
12:00
18:00
Time of Day (LTC)

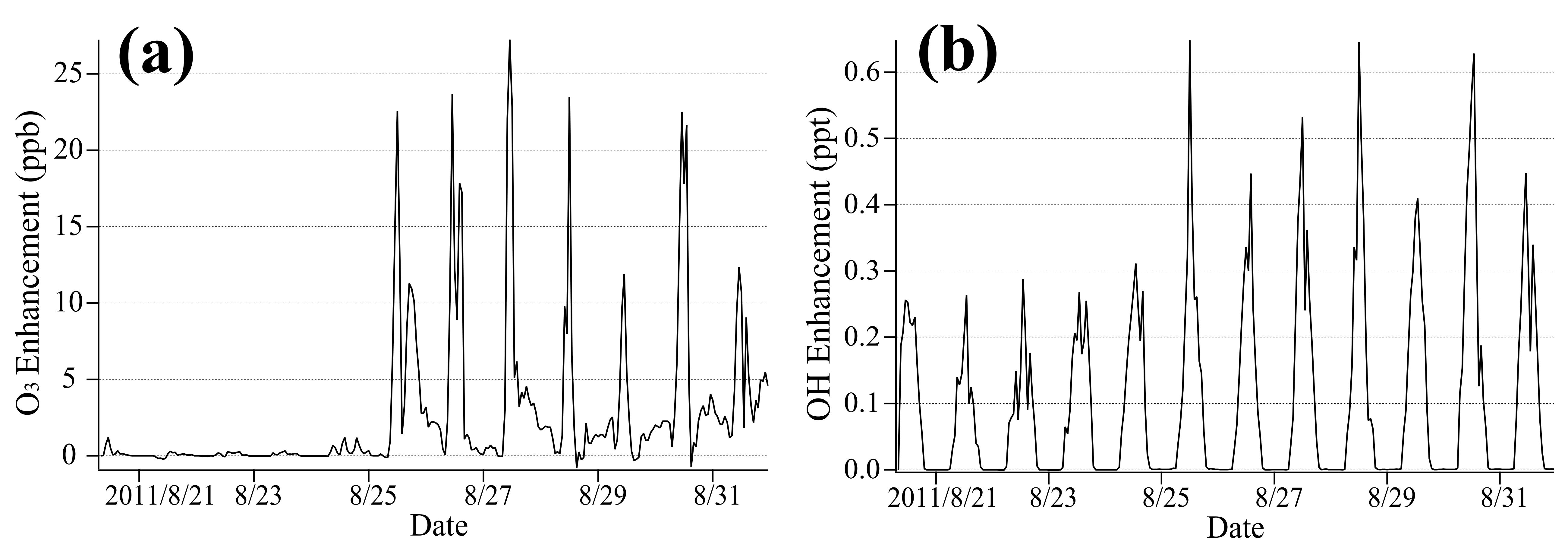

(a)
O3 Enhancement (ppb)
25
20
15
10
5
0
2011/8/21
8/23
8/25
8/27
8/29
8/31
Date
(b)
OH Enhancement (ppt)
0.6
0.5
0.4
0.3
0.2
0.1
0.0
2011/8/21
8/23
8/25
8/27
8/29
8/31
Date

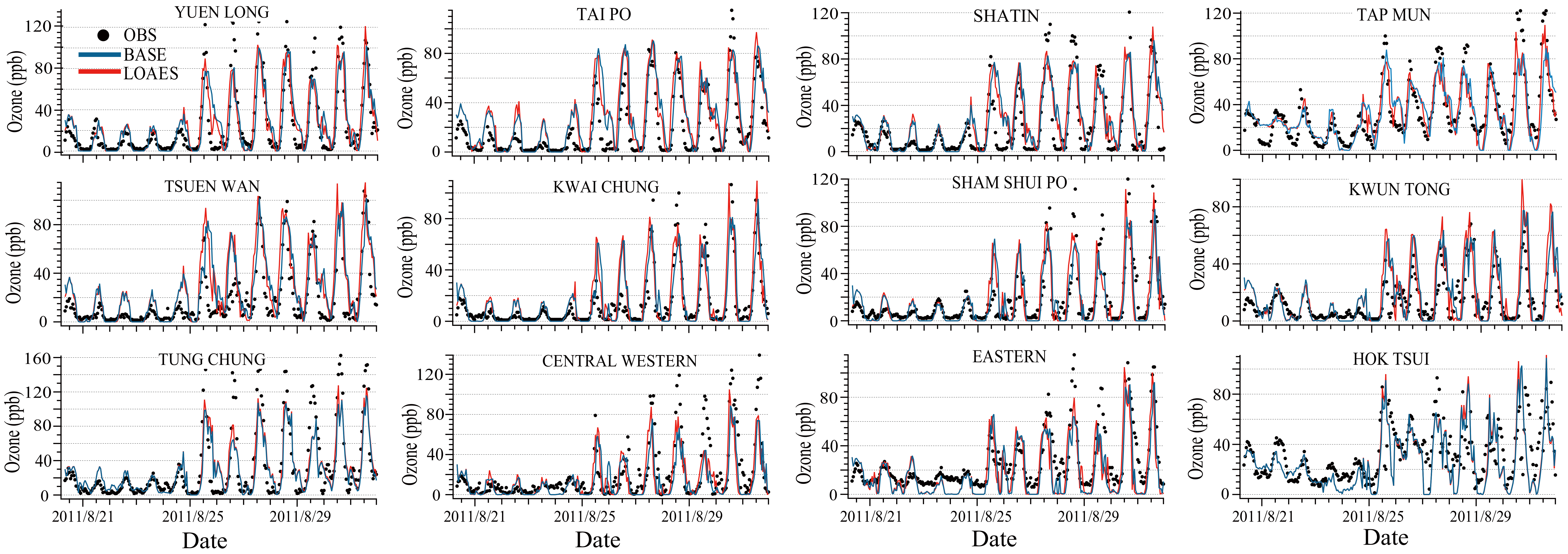

YUEN LONG
OBS
BASE
LOAES
TAI PO
SHATIN
TAP MUN
TSUEN WAN
KWAI CHUNG
SHAM SHUI PO
KWUN TONG
TUNG CHUNG
CENTRAL WESTERN
EASTERN
HOK TSUI
Ozone (ppb)
2011/8/21
2011/8/25
2011/8/29
Date

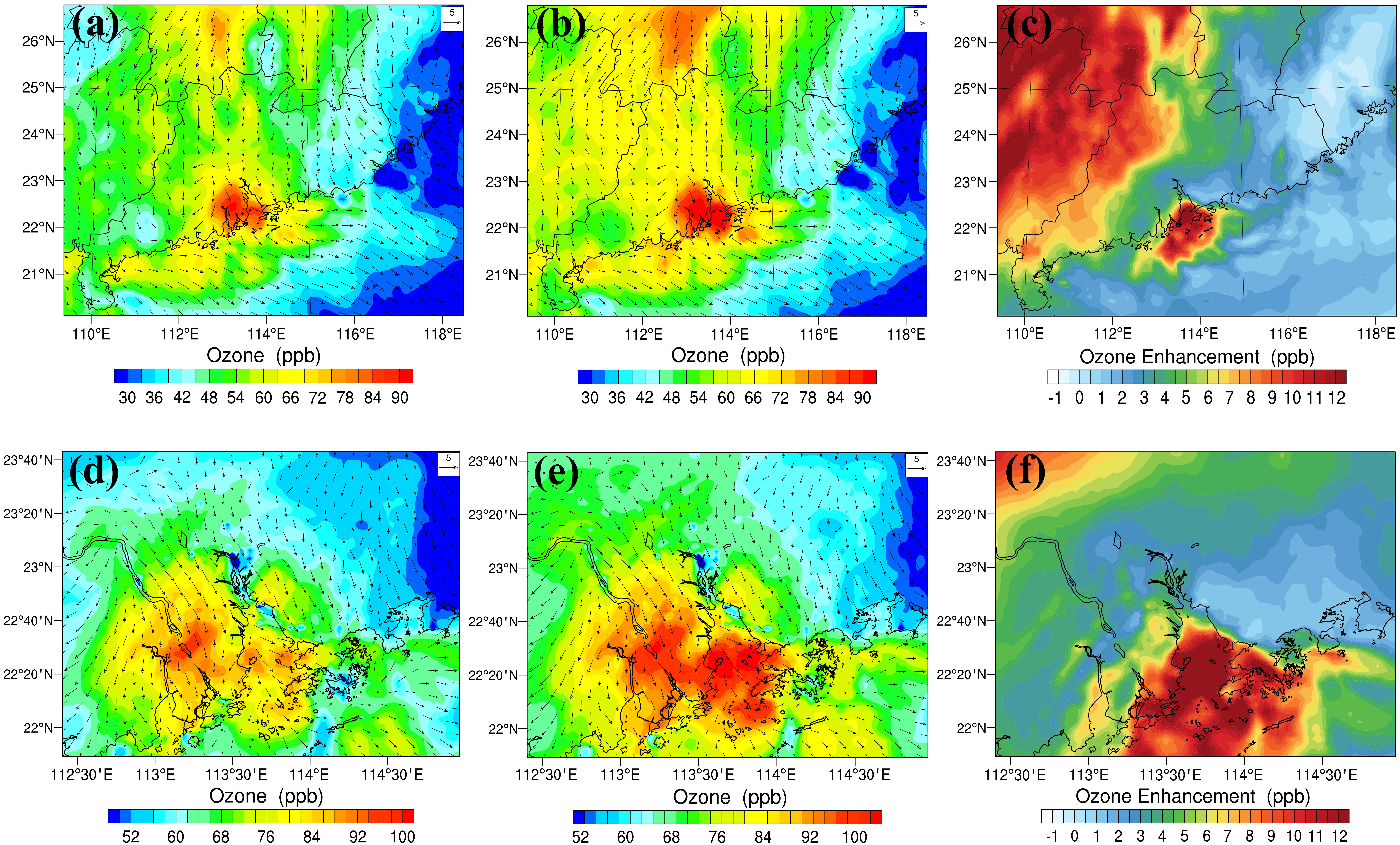
(a)
(b)
(c)
(d)
(e)
(f)
26°N
25°N
24°N
23°N
22°N
21°N
110°E
112°E
114°E
116°E
118°E
Ozone (ppb)
30 36 42 48 54 60 66 72 78 84 90
Ozone Enhancement (ppb)
-1 0 1 2 3 4 5 6 7 8 9 10 11 12
23°40'N
23°20'N
23°N
22°40'N
22°20'N
22°N
112°30'E
113°E
113°30'E
114°E
114°30'E
52 60 68 76 84 92 100
5